Stem Cell Reports
Article
ISSCR
OPEN ACCESS

Early reactivation of clustered genes on the inactive X chromosome during somatic cell reprogramming

Shiho Aizawa,[1] Ken Nishimura,[1,*] Gonzalo Seminario Mondejar,[1] Arun Kumar,[1] Phuong Linh Bui,[1] Yen Thi Hai Tran,[1] Akihiro Kuno,[2,3] Masafumi Muratani,[4] Shin Kobayashi,[5] Tsukasa Nabekura,[6,7,8] Akira Shibuya,[6,7,8] Eiji Sugihara,[9,10] Taka-Aki Sato,[9] Aya Fukuda,[1] Yohei Hayashi,[11] and Koji Hisatake[1,*]

[1]Laboratory of Gene Regulation, Faculty of Medicine, University of Tsukuba, 1-1-1 Tennodai, Tsukuba, Ibaraki 305-8575, Japan
[2]Laboratory of Animal Resource Center, Department of Anatomy and Embryology, Faculty of Medicine, University of Tsukuba, 1-1-1 Tennodai, Tsukuba, Ibaraki 305-8575, Japan
[3]Ph.D. Program in Human Biology, School of Integrative and Global Majors, University of Tsukuba, Tsukuba, Ibaraki 305-8575, Japan
[4]Department of Genome Biology, Faculty of Medicine, University of Tsukuba, 1-1-1 Tennodai, Tsukuba, Ibaraki 305-0006, Japan
[5]Cellular and Molecular Biotechnology Research Institute, National Institute of Advanced Industrial Science and Technology, 2-4-7 Aomi, Koutou-ku, Tokyo 135-0064, Japan
[6]Department of Immunology, Faculty of Medicine, University of Tsukuba, 1-1-1 Tennodai, Tsukuba, Ibaraki 305-8575, Japan
[7]Life Science Center for Survival Dynamics, Tsukuba Advanced Research Alliance, University of Tsukuba, 1-1-1 Tennodai, Tsukuba, Ibaraki 305-8575, Japan
[8]R&D Center for Innovative Drug Discovery, University of Tsukuba, 1-1-1 Tennodai, Tsukuba, Ibaraki 305-8575, Japan
[9]Research and Development Center for Precision Medicine, Innovation Medical Research Institute, University of Tsukuba, 1-2 Kasuga, Tsukuba, Ibaraki 305-8550, Japan
[10]Center for Joint Research Facilities Support, Research Promotion and Support Headquarters, Fujita Health University, Toyoake, Aichi 470-1192, Japan
[11]iPS Cell Advanced Characterization and Development Team, Bioresource Research Center, RIKEN, 3-1-1 Koyadai, Tsukuba, Ibaraki 305-0074, Japan
*Correspondence: ken-nishimura@md.tsukuba.ac.jp (K.N.), kojihisa@md.tsukuba.ac.jp (K.H.)
https://doi.org/10.1016/j.stemcr.2021.11.008

SUMMARY

Reprogramming of murine female somatic cells to induced pluripotent stem cells (iPSCs) is accompanied by X chromosome reactivation (XCR), by which the inactive X chromosome (Xi) in female somatic cells becomes reactivated. However, how Xi initiates reactivation during reprogramming remains poorly defined. Here, we used a Sendai virus-based reprogramming system to generate partially reprogrammed iPSCs that appear to be undergoing the initial phase of XCR. Allele-specific RNA-seq of these iPSCs revealed that XCR initiates at a subset of genes clustered near the centromere region. The initial phase of XCR occurs when the cells transit through mesenchymal-epithelial transition (MET) before complete shutoff of *Xist* expression. Moreover, regulatory regions of these genes display dynamic changes in lysine-demethylase 1a (KDM1A) occupancy. Our results identified clustered genes on the Xi that show reactivation in the initial phase of XCR during reprogramming and suggest a possible role for histone demethylation in this process.

INTRODUCTION

Derivation of induced pluripotent stem cells (iPSCs) from somatic cells by introduction of key pluripotency transcription factors offers tremendous potential for regenerative medicine, disease modeling, drug development, and understanding fundamental mechanisms of how cells determine their identities (Takahashi and Yamanaka, 2013). Cell identity is governed by a defined pattern of gene expression, which is underpinned by various epigenetic mechanisms (Barrero et al., 2010). As such, somatic cell reprogramming serves as an excellent model system to unravel epigenetic mechanisms that determine cell identity. One of the most drastic epigenetic changes during reprogramming is reactivation of the inactive X chromosome (XCR) in mammalian female somatic cells (Pasque and Plath, 2015). XCR is the reversal of X chromosome inactivation (XCI), which occurs during differentiation of cells in the inner cell mass (ICM) of female embryos. Because iPSCs are equivalent to embryonic stem cells (ESCs) derived from the ICM, conversion of female somatic cells into iPSCs evokes XCR when iPSCs acquire the naive pluripotent state (Nichols and Smith, 2009).

XCI and XCR involve chromosome-wide epigenetic changes during early embryonic development of female eutherian mammals. In the mouse, the paternal X chromosome undergoes imprinted XCI by the action of a non-coding RNA, *Xist*, at the cleavage stage (Okamoto et al., 2004) and is subsequently reactivated in the ICM of the blastocyst (Sado et al., 2001). Then ICM cells randomly choose one of the two active X chromosomes for inactivation (Lyon, 1961). The chosen X chromosome initiates expression of *Xist*, which subsequently spreads to coat the whole X chromosome and eventually inactivates genes on the X chromosome (Engreitz et al., 2013; Simon et al., 2013), except for escapee genes that are not subject to XCI (Brown et al., 1991). The inactive X chromosome is maintained stably by H3K27me3 and DNA methylation throughout subsequent cell divisions (Csankovszki et al., 2001).

In contrast to XCI, which is recapitulated by *in vitro* differentiation of female ESCs, XCR poses a major challenge for its mechanistic understanding due to lack of an

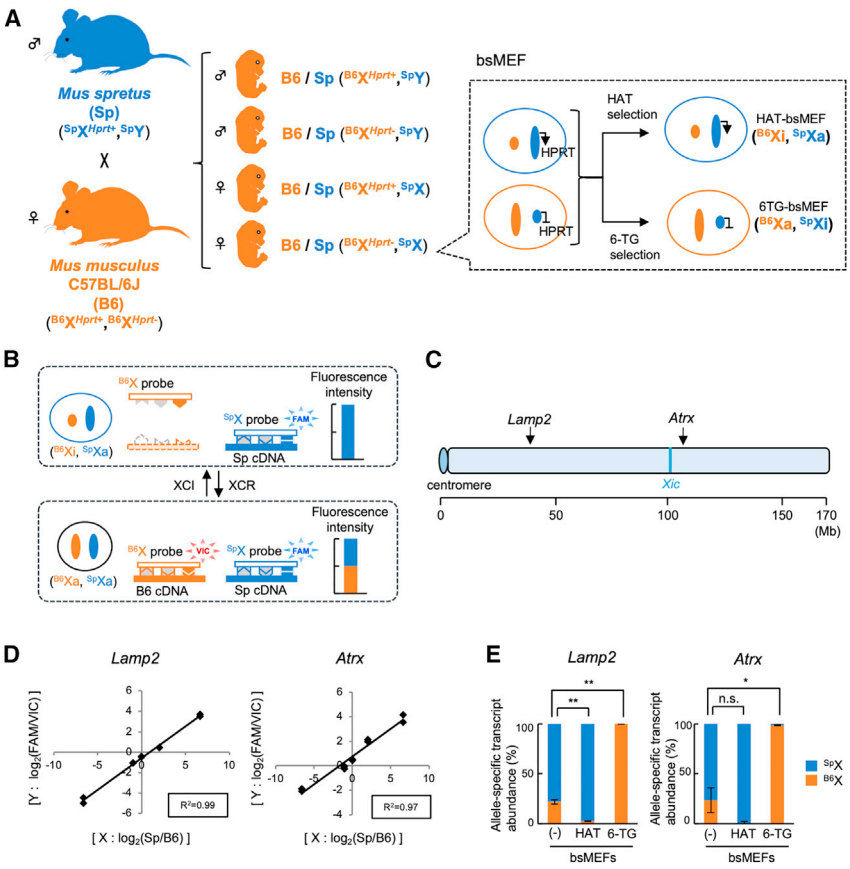

Figure 1. Establishment of a TaqMan-based system to quantify allele-specific transcripts from the X chromosomes

(A) Isolation of hybrid MEFs for XCR analyses.

(B) TaqMan probes that discriminate transcripts from B6 and Sp alleles. TaqMan probes in a single reaction recognize their cognate allele-specific transcripts, which differ by SNPs or an MNP, and emit fluorescence (VIC or FAM).

(C) Mouse X chromosome showing the locations of *Lamp2*, *Atrx*, and the X-inactivation center (Xic).

(D) Linear correlation between the ratio of the allele-specific cDNA amounts and the ratio of emitted fluorescence for each allele. cDNAs derived from homozygous B6 and Sp mice were mixed at five different ratios, and qRT-PCR was performed using TaqMan probes for the *Lamp2* or *Atrx* gene. The square of the correlation coefficient is indicated by R^2.

(E) Relative abundance of allele-specific transcripts in drug-selected MEFs. The relative abundances of allele-specific transcripts in HAT- or 6-TG-selected bsMEFs were calculated by using TaqMan probes for *Lamp2* or *Atrx*. Data represent mean ± SEM of at least three independent experiments. *$p < 0.05$ and **$p < 0.01$. n.s., not significant.

appropriate *in vitro* system. However, XCR has been observed in several experimental systems in which somatic cells or nuclei are reprogrammed into the pluripotent state. XCR has been reported to occur in somatic cell nuclear transfer (Eggan et al., 2000), cell fusion between somatic cells and pluripotent cells (Takagi et al., 1983), and transcription factor-mediated reprogramming of somatic cells to iPSCs (Maherali et al., 2007). Studies using mouse embryos and *in vitro* reprogramming systems revealed a close link between XCR and pluripotency (Maherali et al., 2007). Besides the negative effect of *Xist* on XCR (Pasque et al., 2014), only a small number of factors are known to play a role in XCR. For example, *Tsix* and PRDM14 promote XCR, whereas KDM6A (also known as UTX) and HDACs delay XCR (Talon et al., 2019). A more recent study that used allele-specific RNA sequencing (RNA-seq) revealed that genes on the Xi become progressively reactivated during reprogramming (Janiszewski et al., 2019). However, the earliest events of XCR during reprogramming remain poorly defined.

We previously developed a somatic cell reprogramming system based upon replication-defective and persistent Sendai virus (SeVdp) vector (Nishimura et al., 2011). An SeVdp-derived reprogramming vector, SeVdp(fK-OSM), expresses OCT4, SOX2, KLF4, and c-MYC, and its KLF4 is tagged with a destabilization domain (DD). DD promotes degradation of the tagged KLF4, and the amount of KLF4 expressed from the vector is controllable by Shield1, a chemical inhibitor of the DD function (Nishimura et al., 2014). Depending upon the amount of Shield1 added to the culture, SeVdp (fK-OSM) converts somatic cells into iPSCs that have been reprogrammed to different extents. These partially reprogrammed iPSCs remain relatively stable and easily expandable (Nishimura et al., 2014). In this study, we used a series of partially reprogrammed iPSCs and investigated the early events of XCR during reprogramming.

RESULTS

A TaqMan-based system to detect allele-specific transcripts from the X chromosome

To study early events of XCR during reprogramming, we set out to establish a convenient system to monitor allele-specific transcripts from the Xi. First, we produced hybrid embryos by crossing male *Mus spretus* (Sp) and female *Mus musculus domesticus* C57BL/6J (B6) that carried a mutant *Hprt* allele (Figure 1A). *Mus spretus* and *Mus musculus* strains

diverged more than 1.5 million years ago and thus show one sequence variant every 50–130 bases (Mahler et al., 2008; Zhang et al., 2005). Thus, hybrid cells between the two strains would possess many single-nucleotide polymorphisms (SNPs), multiple-nucleotide polymorphisms (MNPs), and indels, which are available for distinguishing allele-specific transcripts. On the basis of genome analysis of the hybrid embryos, we chose females that carried the mutant *Hprt* allele to obtain mouse embryonic fibroblasts (MEFs) (Figure 1A). The obtained MEFs, termed bsMEFs, were then selected with hypoxanthine-aminopterin-thymidine (HAT) or 6-thioguanine (6-TG) to isolate cells that carried a *Mus musculus*-derived X chromosome in an inactive (^{B6}Xi) or active (^{B6}Xa) form, respectively (Figure 1A). The selected cells were confirmed by allele-specific digestion patterns of the amplified *Lamp2* transcripts from the X chromosome (Figures S1A and S1B).

We then searched a database of the Mouse Genomes Project at the Wellcome Sanger Institute (https://www.sanger.ac.uk/data/mouse-genomes-project/) for polymorphisms to design TaqMan probes that distinguish allele-specific transcripts from Sp and B6 X chromosomes (Figure 1B). Among the tested TaqMan probes, those for *Lamp2* and *Atrx*, which included transversion in one MNP and two SNPs, respectively, were found to discriminate alleles quantitatively (Figures 1C, 1D, S1C, and S1D). These probes enabled quantitative estimation of allele-specific transcripts in highly correlative linear ranges (R^2 > 0.9), which approached 2 orders of magnitude (Figures 1D and S1E). The allele-specific transcript analyses showed that unselected bsMEFs exhibited a skewed XCI, with 70%–75% of the cells possessing an active Sp X chromosome (^{Sp}Xa) (Figure 1E). In addition, HAT or 6-TG selection highly enriched MEFs with ^{B6}Xi and ^{Sp}Xa (HAT-bsMEFs) or with ^{B6}Xa and ^{Sp}Xi (6TG-bsMEFs), respectively (Figures 1A and 1E). Thus, the TaqMan probes encompassing either a single MNP or two SNPs enable quantification of allele-specific transcripts from the *Lamp2* and *Atrx* genes, providing a quick, sensitive means to capture low-level transcripts from the Xi during reprogramming.

Partially reprogrammed iPSCs permit gene expression from the Xi

To generate iPSCs, we used SeVdp(fK-OSM) vector that expresses four reprogramming factors, OCT4, SOX2, c-MYC, and KLF4 (Nishimura et al., 2011). In this vector, KLF4 is fused with a DD, the KLF4 protein level is reduced by ubiquitin-mediated degradation (Banaszynski et al., 2006), and the KLF4 level is adjustable by the amount of added Shield1 (Nishimura et al., 2014) (Figure 2A). Indeed, addition of 100 nM Shield1 practically prevents KLF4 degradation and reprograms MEFs to the fully pluripotent state. Without Shield1, however, the KLF4 level is reduced to ~30%, and reprogramming virtually stalls at an intermediate stage (Nishimura et al., 2014). Addition of 30 nM Shield1 increases the KLF4 level to ~70% and allows reprogramming to a more advanced stage before stalling (Nishimura et al., 2014). Although these partially reprogrammed iPSCs are relatively stable in the SeVdp(fK-OSM) system (Nishimura et al., 2014), we noted that prolonged culture allowed them to progress in reprogramming, albeit at a markedly slower rate.

We reprogrammed HAT-bsMEFs by using SeVdp(fK-OSM) with 100 nM Shield1 (High-K) to generate iPSCs that express endogenous *Oct4*, *Nanog*, and *Rex1* at high levels (Figure S2A). These fully reprogrammed iPSCs expressed *Lamp2* and *Atrx* from ^{B6}Xi (Figures S2B), with clear downregulation of *Xist* (Figure S2C). However, the ^{B6}X-specific transcripts often surpassed the cognate ^{Sp}X-specific transcripts at this stage of reprogramming (Figure S2B). This suggests that loss of an X chromosome (Pasque et al., 2018), a secondary XCI (Kim et al., 2014), or erosion of Xa (Vallot et al., 2015) may have occurred when iPSCs reached the fully pluripotent state. A similar phenomenon was also observed when we reprogrammed female MEFs derived from Momiji mice, which carries mCherry and EGFP at the *Hprt* locus (Kobayashi et al., 2016). When mCherry(+)/EGFP(−) MEFs were reprogrammed with SeVdp(fK-OSM) at 100 nM Shield1, 81.4% and 93.2% of the cells became mCherry(+)/EGFP(+) at days 30 and 37, respectively, which indicates that XCR occurred in these cells (Figures S2D and S2E). However, a substantial faction of cells lost expression of either mCherry or EGFP at day 44 (Figure S2E).

Given the instability of XCR when iPSCs were fully reprogrammed, we sought to focus on the earlier phase of XCR, which appeared to have initiated by day 30 of reprogramming under the High-K condition (Figure S2E). To obtain iPSCs at earlier stages, we reprogrammed MEFs without Shield1 or with 30 nM Shield1 (Figure 2A). When HAT-bsMEFs were reprogrammed by SeVdp(fK-OSM) without Shield1 (Low-K) or with 30 nM Shield1 (Mid-K) for 43 days, the cells progressed to intermediate stages and expressed various pluripotency markers, including *Fbxo15*, *Nodal*, *Nr5a2*, *Utf1*, endogenous *Oct4*, *Nanog*, and *Rex1*, at low or moderate levels (Figure 2B) (Nishimura et al., 2014). Low-K cells expressed low levels of *Lamp2* from the Xi at day 34, and Mid-K cells expressed significant levels of *Lamp2* at days 26 and 34. Both Low-K cells and Mid-K cells failed to express *Atrx* from the Xi until day 43 (Figure 2C). Low-K cells showed no significant *Xist* downregulation throughout reprogramming, whereas Mid-K cells showed *Xist* downregulation at day 43 (Figure S2F). These results suggest that some genes on the Xi may become reactivated at an early reprogramming stage, before acquisition of full pluripotency during reprogramming.

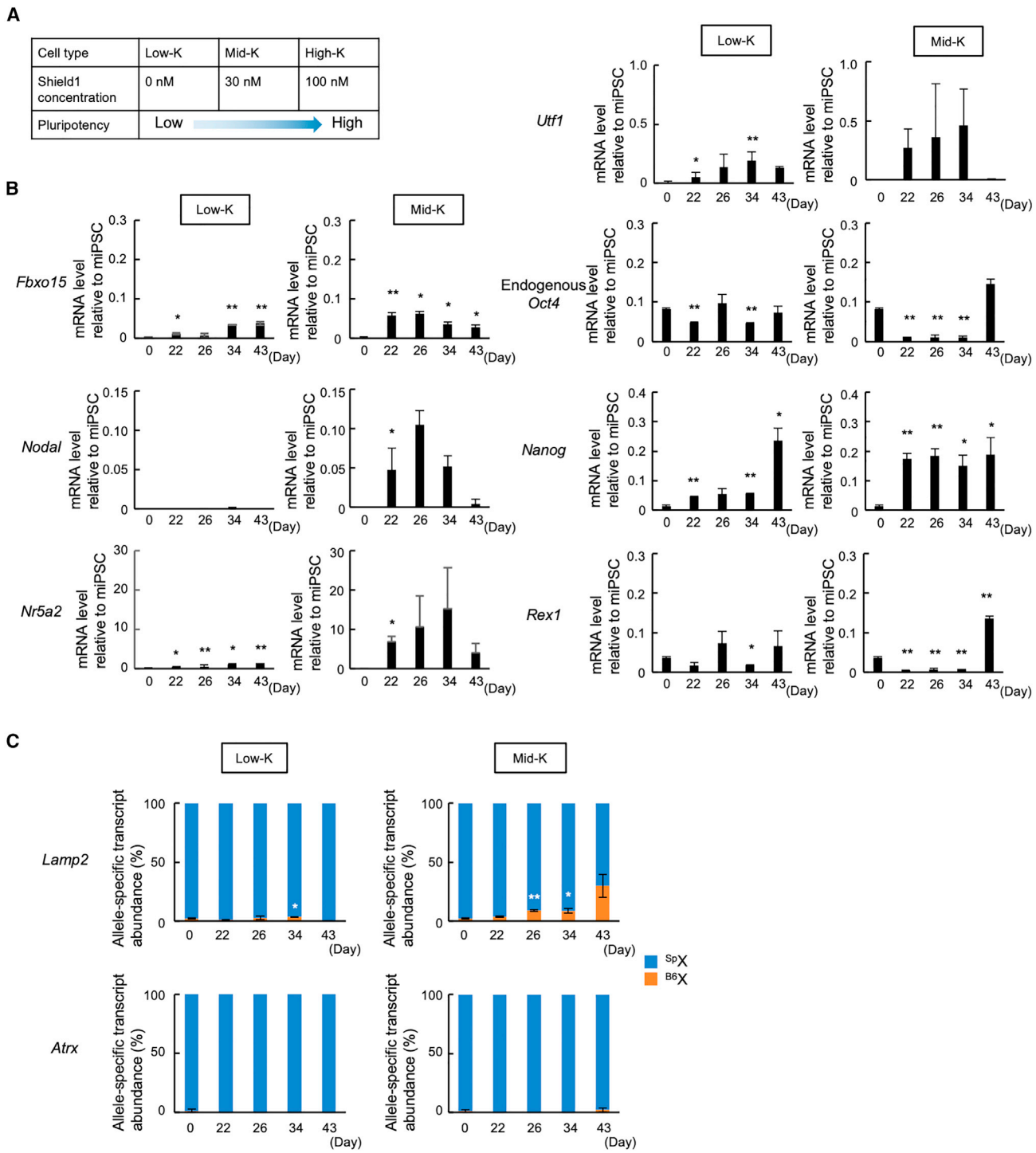

Figure 2. Reactivation of X-linked genes from the Xi in partially reprogrammed iPSCs

(A) Generation of iPSCs with different pluripotency levels (Low-K, Mid-K, and High-K) by SeVdp(fK-OSM) in the presence of different Shield1 concentrations.

(B) Expression kinetics of pluripotency markers in partially reprogrammed iPSCs. HAT-bsMEFs were reprogrammed under the Low-K and Mid-K conditions. The expression levels of indicated genes were determined by qRT-PCR at indicated days of reprogramming.

(C) Relative abundances of allele-specific transcripts of *Lamp2* and *Atrx* in HAT-bsMEFs reprogrammed under the Low-K and Mid-K conditions. The same cells prepared in (B) were analyzed for qRT-PCR using TaqMan probes.

All data represent mean ± SEM of at least three independent experiments. *$p < 0.05$ and **$p < 0.01$ versus HAT-bsMEFs (day 0).

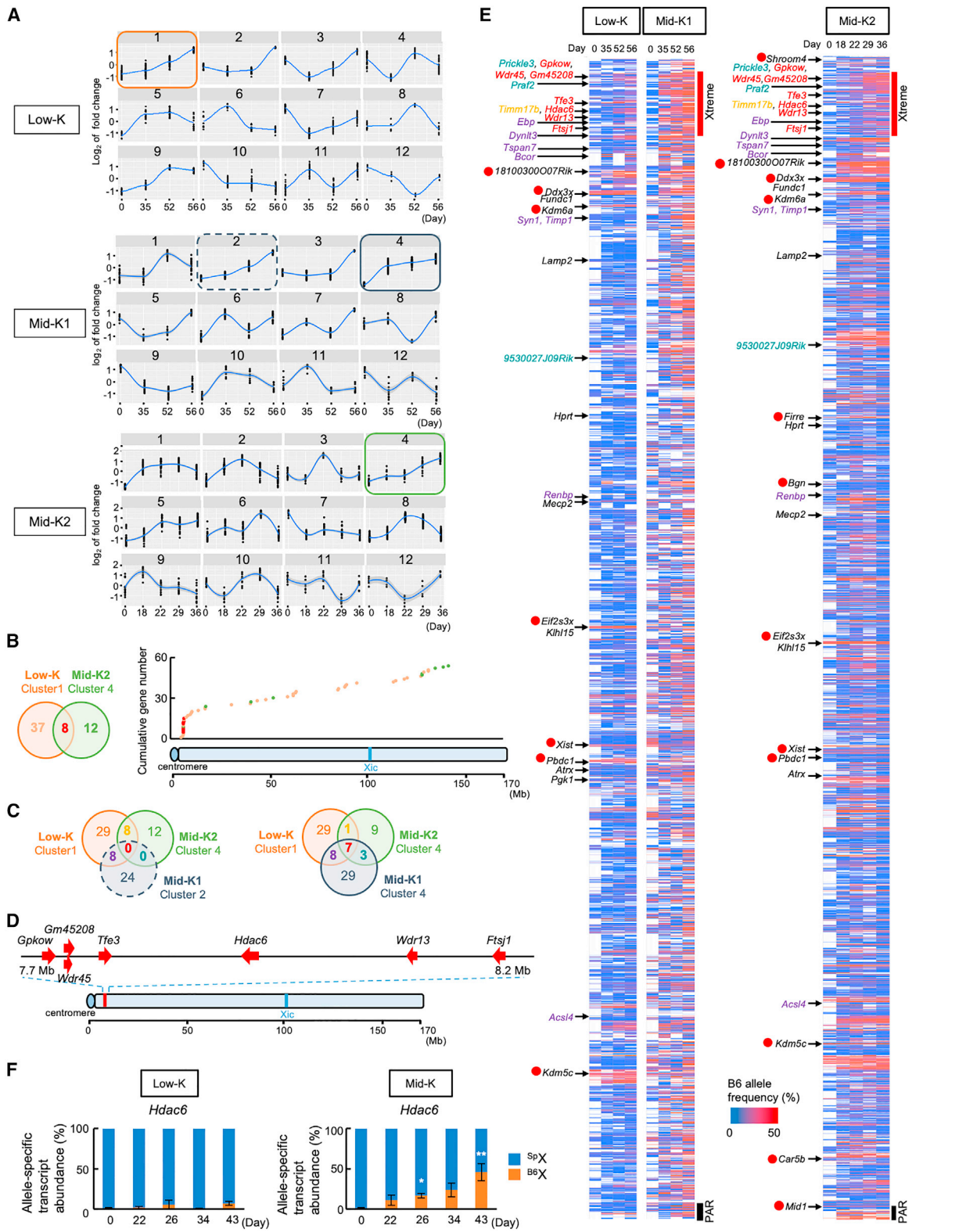

(legend on next page)

A subset of genes exhibits early-onset reactivation from the Xi during reprogramming

To obtain a comprehensive view of chromosome-wide gene reactivation from the Xi at intermediate stages, we performed RNA-seq analysis of Low-K and Mid-K (hereafter termed Mid-K1) cells at different time points of reprogramming (up to day 56). Besides Mid-K1 cells, we prepared Mid-K2 cells reprogrammed for a shorter period (up to day 36) because Mid-K1 cells had already expressed *Lamp2* by day 35 (Figure S3A). The expression of *Lamp2* expression from the Xi (Figure S3A) and pluripotency markers (Figure S3B) showed that Mid-K2 cells are intermediate between Low-K and Mid-K1 cells. After RNA-seq of Low-K, Mid-K1, and Mid-K2 cells, the X-linked transcript reads encompassing SNPs, MNPs, and indels were assigned to either B6 or Sp X chromosome. Then, the B6- or Sp-specific transcripts were annotated to more than 400 X-linked genes to quantitatively assess the relative level of ^{B6}Xi-specific transcripts (Figure S4A).

Throughout the analyzed periods of reprogramming, alleles on the Xa showed relatively constant expression levels, whereas those on the Xi showed little or low expression except for escapee genes (Figure S4B). First, we categorized gene expression patterns of ^{B6}Xi-specific transcripts into 12 distinct clusters in an unbiased manner. Low-K cluster 1, Mid-K1 clusters 2 and 4, and Mid-K2 cluster 4 included genes that gradually increased expression throughout reprogramming (Figure 3A). Eight genes in the overlap of Low-K cluster 1 and Mid-K2 cluster 4 were localized to the region proximal to the centromere (Figure 3B). Seven of them were also included in Mid-K1 cluster 4 but none in Mid-K1 cluster 2 (Figure 3C). Thus, *Gpkow*, *Wdr45*, *Gm45208*, *Tfe3*, *Hdac6*, *Wdr13*, and *Ftsj1* are shared among the three clusters and localized near the centromere of the X chromosome (Figure 3D).

We then calculated the relative levels of the Xi-specific transcripts against the Xa-specific transcripts at different time points of Low-K, Mid-K1, and Mid-K2 cells to generate heatmaps. As evident in Figure 3E, reactivation of genes on the Xi occurred earlier near the centromere region than in other regions. This region corresponds to the same 7.7–8.2 Mb region identified by clustering gene expression patterns (Figure 3C) and includes *Gpkow*, *Wdr45*, *Gm45208*, *Tfe3*, *Hdac6*, *Wdr13*, and *Ftsj1* (Figure 3D). These genes initiated expression from the Xi when the mesenchymal markers (*Cdh2*, *Snai1*, *Zeb2*, and *Twist1*) were downregulated and epithelial markers (*Cdh1*, *Ocln*, and *Epcam*) were upregulated, which indicates an ongoing mesenchymal-epithelial transition (MET) (Skrypek et al., 2017) (Figure S4C). In addition, early-onset reactivation was confirmed more quantitatively by a TaqMan probe for *Hdac6* (Figures 3F and S1D), which showed a similar expression profile to that by RNA-seq data (Figure 3E). By contrast, genes expressed from the Xi in HAT-bsMEFs included escapee genes (*Shroom4*, *1810030O07Rik*, *Ddx3x*, *Kdm6a*, *Firre*, *Bgn*, *Eif2s3x*, *Xist*, *Pbdc1*, *Kdm5c*, *Car5b*, and *Mid1*), which are defined as genes that show at least 10% expression from the Xi versus Xa (Figure 3E) and reported as escapee genes by others (Brown et al., 1991; Carrel and Willard, 2005). Given that the seven genes that show early-onset reactivation were clustered in a ~0.5 Mb region, we named the region Xtreme (X-transcriptional reactivation manifesting element).

Single-cell analysis of early-onset reactivation from the Xi during reprogramming

To further confirm early-onset reactivation of genes in the Xtreme region, we used Mid-K cells to analyze *Hdac6* reactivation on the Xi at single-cell resolution. MEFs were reprogrammed in the presence of 30 nM Shield1 for 26 or

Figure 3. Expression profiles of the genes on the Xi during reprogramming

(A) Clustering of expression patterns of genes reactivated on the Xi. X-linked genes were assigned into 12 clusters by expression patterns in Low-K, Mid-K1, or Mid-K2 cells. The colored squares indicate clusters that show a trajectory of increasing expression.

(B) X chromosomal locations of the genes that show increasing expression and are shared between Low-K and Mid-K2. A Venn diagram shows overlapping genes between Low-K cluster 1 and Mid-K2 cluster 4 (left panel), and a scatter diagram shows distribution of the all genes included in Low-K cluster 1 and Mid-K2 cluster 4 (right panel). The colors of dots in the scatter diagram reflect the ones in the Venn diagram.

(C) Venn diagrams show overlapping genes among Low-K cluster 1, Mid-K2 cluster 4, and Mid-K1 cluster 2 (left) as well as those among Low-K cluster 1, Mid-K2 cluster 4, and Mid-K1 cluster 4 (right).

(D) Locations of the seven genes that show early-onset reactivation.

(E) Heatmaps of transcriptional reactivation of the genes on the Xi chromosome. B6 allele frequencies in each polymorphic position were ordered by their genomic locations on the X chromosome. The genes that are common in among Low-K cluster 1, Mid-K2 cluster 4, and Mid-K1 cluster 4 are colored in yellow (one gene), red, (seven genes), purple (eight genes), and green (three genes), as in the right diagram in (C). Genes regarded as escapee genes are marked with red circles. Xtreme region and pseudoautosomal region (PAR) are shown with red and black lines, respectively.

(F) Relative abundances of allele-specific transcripts of *Hdac6* in HAT-bsMEFs reprogrammed under the Low-K and Mid-K conditions. The same cells prepared in Figure 2B were analyzed.

Data represent mean ± SEM of at least three independent experiments. *$p < 0.05$ and **$p < 0.01$ versus HAT-bsMEFs (day 0).

34 days, and the cells were sorted using fluorescence-activated cell sorting (FACS) to obtain single cells. RNA was prepared from each cell and used to generate cDNA by reverse transcription with random displacement amplification (RT-RamDA), a method that captures transcriptome in single cells with high sensitivity (Hayashi et al., 2018). The cDNA was then used to detect allele-specific expression of *Hdac6*, *Lamp2*, and *Atrx* by the TaqMan-based method (Figure 4A). In addition, *Xist* expression in each cell was determined using qPCR of the cDNA (Figure 4A). At day 26 of reprogramming, 44% of the cells were *Hdac6*(+) and *Lamp2*(−), whereas 6% were *Hdac6*(−) and *Lamp2*(+). At day 34, 62% of the cells were *Hdac6*(+) and *Lamp2*(−), whereas 15% were *Hdac6*(−) and *Lamp2*(+) (Figure 4B, upper panels). These results show that *Hdac6* has tendency to be reactivated earlier than *Lamp2* from the Xi during reprogramming. Comparison of *Hdac6* and *Atrx* also showed that *Hdac6* is reactivated earlier than *Atrx* on the Xi (Figure 4B, lower panels). Using single-cell analysis, we also analyzed the relationship between *Xist* expression and *Hdac6* reactivation on the Xi. At days 26 and 34 of reprogramming, 25% and 31% of the cells showed reactivation of *Hdac6* while still expressing *Xist* (Figure 4C). However, in the cells that expressed both *Hdac6* and *Xist* on the Xi, *Xist* expression was clearly reduced (Figure S5). As shown in Figure 4D, *Hdac6*, *Lamp2*, and *Atrx* were expressed from the Xi in 57%, 43%, and 0% of the *Xist*(+) cells at day 26, respectively. At day 34, *Hdac6*, *Lamp2*, and *Atrx* were expressed from the Xi in 67%, 17%, and 50% of the *Xist*(+) cells, respectively. Thus, *Lamp2* and *Atrx* were also reactivated on the Xi in the cells expressing *Xist*. Collectively, these single-cell analyses confirm that *Hdac6* in the Xtreme region tends to be reactivated earlier than *Lamp2* and *Atrx* during reprogramming. In addition, a substantial fraction of cells shows reactivation of genes on the Xi even when *Xist* is still present.

Identification of factors required for early-onset reactivation on the Xi

To find structural features of the Xtreme region, we reanalyzed the assay for transposase-accessible chromatin (ATAC) sequencing data of the Xi chromosome in hybrid female cells between *M. m. domesticus* and *M. m. castaneus* (Giorgetti et al., 2016). We found that the Xtreme region on the Xi adopts a more accessible structure compared with the whole Xi (Figure 5A). In addition, Figure 5B shows that the chromatin accessibility of the Xtreme region is comparable with regions containing escapees, *1810030O07Rik*, *Firre*, *Bgn*, *Xist*, *Pbdc1*, *Kdm5c*, *Car5b*, and *Mid1* (Yang et al., 2010). Moreover, the Xtreme region is one of the gene-rich regions on the X chromosome and forms a single TAD (topologically associating domain) in ESCs (Marks et al., 2015). These findings suggest that the Xtreme region on the Xi chromatin may be relatively accessible for transcriptional regulators during an early stage of reprogramming.

To screen for such factors that might gain access to the Xtreme region and function in the reactivation of the genes during an early stage of reprogramming, we used the ChIP-Atlas database (Oki et al., 2018), which includes 332 transcriptional regulators that have been experimentally confirmed to occupy the regulatory regions within the Xtreme region in ESCs. We searched for factors that show occupancy within the 1 kb of the transcription start sites (TSSs) of *Gpkow*, *Gm45208*, *Wdr45*, *Tfe3*, *Hdac6*, *Wdr13*, and *Ftsj1* genes (Figures 5C and S6A–S6C), all of which show early-onset reactivation on the Xi during reprogramming (Figure 3D). Five transcriptional regulators, KDM1A, KDM4C, NELFA, TCF12, and OTX2, were found to occupy the regulatory regions of at least five of the seven genes in the Xtreme region (Figures 5C and S6A–S6C).

To confirm their involvement in early-onset reactivation of the genes on the Xi, we knocked down each candidate gene by short hairpin RNAs (shRNAs) expressed from silencing-resistant retrovirus vectors (Figures S6D–S6G) and reprogrammed the cells with SeVdp(fK-OSM) with 30 nM Shield1. After 20 days of reprogramming, almost no reactivation of *Hdac6* on the Xi was observed in the cells transduced with a control retrovirus expressing a fluorescent protein, Kusabira-Orange (hKO). However, knockdown of *Kdm1a*, *Nelfa*, or *Otx2* elicited *Hdac6* reactivation to various but statistically significant extents (Figure 5D). By contrast, *Lamp2* and *Atrx* were not reactivated on the Xi at this stage of reprogramming (Figure 5E). Importantly, expression of shRNA for *Kdm1a*, *Nelfa*, or *Otx2* showed only minor effects on the expression levels of pluripotency markers such as endogenous *Oct4*, *Nanog*, and *Rex1* (Figure 5F), indicating that knockdown of *Kdm1a*, *Nelfa*, or *Otx2* may facilitate *Hdac6* reactivation even when they do not promote the reprogramming process. These results suggest a possible role for KDM1A, NELFA and OTX2 in facilitating early-onset reactivation of genes on the Xi.

Dynamic changes of KDM1A occupancy upon reactivation of genes in the Xtreme region of the Xi

Given that the seven genes in the Xtreme region retain relatively accessible chromatin on the Xi (Marks et al., 2015) (Figures 5A and 5B), we hypothesized that these genes may be reactivated via conformational and/or epigenetic regulation of chromatin. We therefore focused on an epigenetic regulator, KDM1A (also known as LSD1), and performed chromatin immunoprecipitation sequencing (ChIP-seq) analysis of HAT-bsMEFs with or without reprogramming under the Low-K or Mid-K conditions. We then determined KDM1A occupancies on the Xi relative to Xa and compared KDM1A occupancies on the seven genes, the Xtreme region, and the whole Xi. Under the Low-K

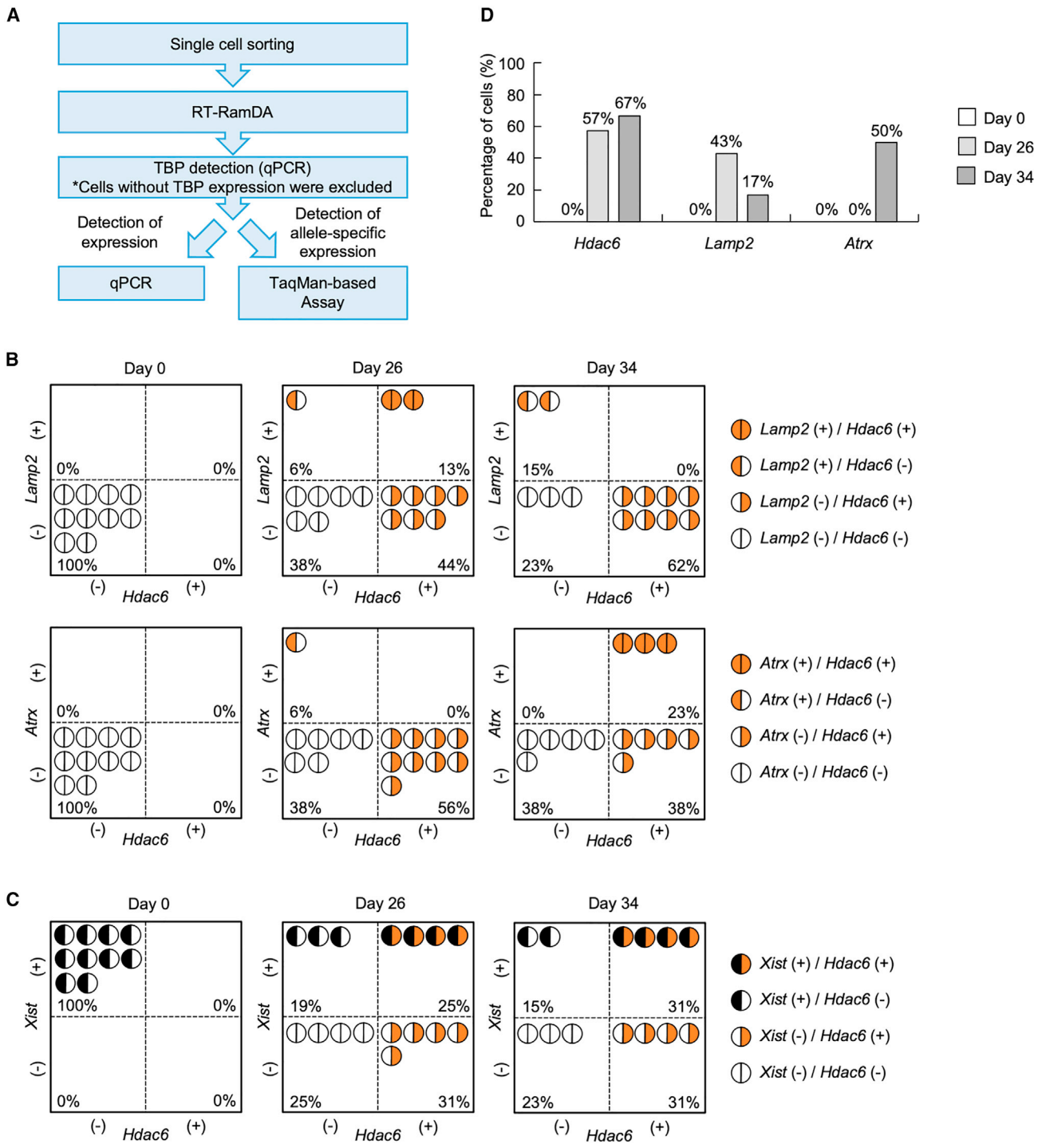

Figure 4. Transcriptional reactivation from the Xi and *Xist* expression in single cells

(A) Flowchart of single-cell analysis to detect *Xist* expression and allele-specific *Lamp2*, *Atrx*, and *Hdac6* transcripts.

(B and C) Patterns of allele-specific gene expression in single cells. Expression of *Hdac6*, *Lamp2*, and *Atrx* from the Xi in single cells was determined using qRT-PCR with TaqMan probes. *Xist* expression was also determined from same cDNAs. Cells were categorized into indicated groups by expression patterns of *Hdac6* and *Lamp2* or *Atrx* (B) or *Hdac6* and *Xist* (C).

(D) Cells that showed *Hdac6*, *Lamp2*, and *Atrx* reactivation with *Xist* expression. The numbers indicate percentages of cells that expressed *Hdac6*, *Lamp2*, or *Atrx* from the Xi in populations of *Xist*-expressing cells.

Raw data are shown in Figure S5.

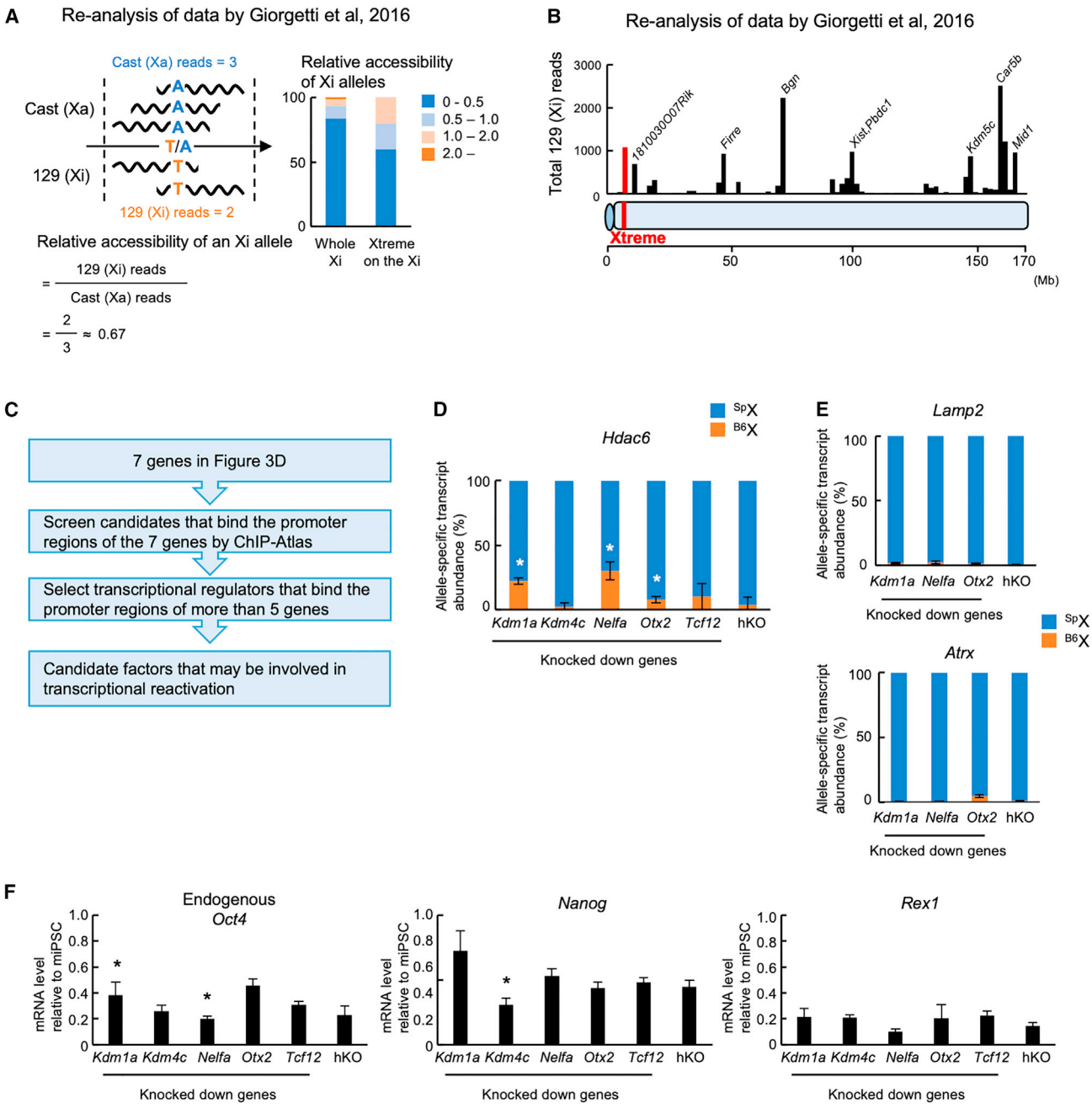

Figure 5. Screening of transcriptional regulators potentially involved in transcriptional reactivation on the Xi

(A) Chromatin accessibility of the Xi chromosome. Left: calculation of relative accessibilities of alleles on the Xi. Right: relative accessibilities of the alleles in the Xtreme region in the Xi. The relative accessibilities of alleles were classified into four groups according to their values. Percentages of the four groups are indicated for the whole Xi or the Xtreme region of the Xi.

(B) Variation in chromatin accessibility in the whole Xi. 129 (Xi) reads that overlap with each polymorphism were summed up in 2 Mbs windows and shown along X chromosome with the Xtreme region and escapee genes.

(C) Flowchart to screen for transcriptional regulators that may be involved in transcriptional reactivation on the Xi.

(D and E) Relative abundance of allele-specific transcripts when the candidate genes were knocked down. After retrovirus-mediated transduction of shRNA against each candidate, HAT-bsMEFs were reprogrammed under the Mid-K condition. Relative abundance of allele-specific transcripts for *Hdac6* (D) or *Lamp2* and *Atrx* (E) were determined at about day 20 of reprogramming.

(legend continued on next page)

condition, KDM1A occupancies on the enhancer, promoter, and gene body of the seven genes increased noticeably compared with the Xtreme region or the whole Xi chromosome (Figure 6A). Under the Mid-K condition, KDM1A occupancy virtually disappeared at the enhancer and promoter regions, concomitant with partial reactivation of *Hdac6* (Figure 6B). Even under this condition, however, KDM1A occupancy at the gene body remained relatively high. Thus, these dynamic changes in KDM1A occupancy suggest a possible physical and/or functional regulation of KDM1A during reactivation in the Xtreme region of the Xi.

To further confirm the role of KDM1A in the reactivation, as indicated by shRNA experiments (Figure 5D), we tested tranylcypromine (TCP), a specific inhibitor of the histone demethylase activity of KDM1A (Sun et al., 2016). HAT-bsMEFs were reprogrammed for 20 days with SeVdp (fK-OSM) in the presence or absence of 5 μM TCP under the Low-K or Mid-K condition. When HAT-bsMEFs were reprogrammed under the Low-K condition, TCP did not enhance expression of *Hdac6* from the Xi (Figure 7A). Under the Mid-K condition, however, TCP significantly enhanced expression of *Hdac6* from the Xi (Figure 7A) but not *Lamp2* and *Atrx2* (Figure 7B), suggesting that inhibition of the histone demethylase activity facilitates reactivation of *Hdac6* on the Xi. Although TCP promotes reprogramming when retrovirus is used for expressing reprogramming factors (Sun et al., 2016), TCP did not promote Sendai virus-mediated reprogramming under the Low-K or Mid-K condition (Figure 7C). Thus, KDM1A inhibition appears to directly reactivate *Hdac6* expression from the Xi rather than via indirect effect through promotion of reprogramming.

DISCUSSION

XCR is observed during female cell reprogramming via introduction of transcription factors into somatic cells (Maherali et al., 2007; Tran et al., 2018) and fusion of somatic cells with ESCs (Tada et al., 2001). These studies underscored a close coupling between XCR and pluripotency, and this coupling is believed to be mediated by the pluripotency factors OCT4, SOX2, and NANOG, which bind the first intron of *Xist* to downregulate its expression (Navarro et al., 2010). However, these studies assessed XCR by relying on fluorescence *in situ* hybridization (FISH) analysis of the *Xist* RNA (Chaumeil et al., 2003) or reactivation of well-studied X-linked genes such as *Pgk1*, *Mecp2*, and *Atrx* (Maherali et al., 2007; Pasque et al., 2014; Tomoda et al., 2012). In our RNA-seq analyses of partially reprogrammed iPSCs, *Pgk1*, *Mecp2*, and *Atrx* are reactivated relatively late during the process of XCR (Figure 3E), suggesting that XCR in previous studies generally designates its completion rather than its initiation.

Although numerous reports indicate a close association between *Xist* shutoff and XCR, it is well known that *Xist* does not play an essential role in maintenance of the Xi (Brown and Willard, 1994; Csankovszki et al., 1999). Moreover, *Xist* is downregulated gradually after acquisition of pluripotency (Do et al., 2008; Kim et al., 2015). Indeed, some genes initiate reactivation on the Xi in the blastocyst even in the presence of *Xist* coating and H3K27me3 (Williams et al., 2011). In nascent primordial germ cells, some X-linked genes initiate biallelic expression before *Xist* expression is shut off, and XCR appears to occur over a prolonged period (Sugimoto and Abe, 2007). During generation of human iPSCs, the Xi undergoes structural changes in the presence of *Xist* coating (Tchieu et al., 2010). Consistent with these observations, our single-cell analysis suggests that complete shutoff of *Xist* is not necessary for initiating gene reactivation on the Xi. However, given that the *Xist* level is reduced to some extent in the cells that showed reactivation of *Hdac6*, *Lamp2*, or *Atrx*, it may be possible that *Xist* is partially removed from the Xi regions where reactivation occurs.

Our analysis of gene expression patterns indicates that some genes in the Xtreme region of the Xi initiate reactivation early when the cells are undergoing MET. This result is in good agreement with a more recent study involving allele-specific RNA sequence analysis of female hybrid cells formed between *M. m. domesticus* and *M. m. castaneus* during reprogramming (Janiszewski et al., 2019). In addition to the findings of Janiszewski et al., we could identify a cluster of genes with early reactivation on the Xi. This may be because we used a sensitive RT-PCR-based TaqMan system to select a series of stable partially reprogrammed iPSCs generated from hybrid cells between *M. m. domesticus* and *M. spretus*. However, our results are based upon partially reprogrammed iPSCs generated by an SeVdp-based vector and therefore warrant further analyses using iPSCs generated by a more commonly used retroviral system.

The Xtreme region is located near the centromere embedded in repressive heterochromatin structure (Kerry, 2014). On the mouse X chromosome, the Xtreme region is farthest from the *Xist* gene, from which *Xist* spreads in

(F) Expression of pluripotency markers in HAT-bsMEFs reprogrammed with knockdown of the candidate genes. Endogenous *Oct4*, Nanog, and Rex1 mRNA levels were determined in the same cells used in (D).

All data represent mean ± SEM of at least three independent experiments. *$p < 0.05$ versus reprogrammed cells with control hKO-expressing retrovirus infection.

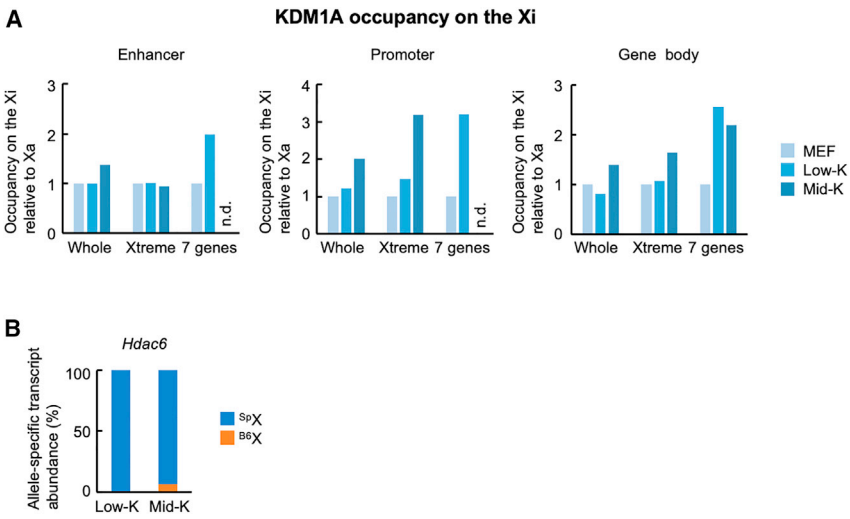

Figure 6. KDM1A occupancy in the Xtreme region

(A) KDM1A occupancy in different XCR states. HAT-bsMEFs were reprogrammed under the Low-K or Mid-K condition for about 20 days. The extracted chromatins were used for allele-specific ChIP-seq for KDM1A. KDM1A occupancies on the Xi relative to its occupancies on the Xa at enhancer, promoter, and gene body are shown. Relative KDM1A occupancies on the Xi in MEFs are set to 1. Seven genes are *Gpkow*, *Wdr45*, *Gm45208*, *Tfe3*, *Hdac6*, *Wdr13*, and *Ftsj1* in the Xtreme region. n.d., not detected.

(B) Relative abundance of allele-specific *Hdac6* transcripts in the cells used for ChIP-seq. Data consist of a single experiment.

two waves to coat the whole X chromosome in *cis* (Simon et al., 2013). More relevantly, the Xtreme region is one of the regions where the gene density is highest on the whole X chromosome (Marks et al., 2015). Thus, the Xtreme region may form a less compact heterochromatin on the Xi. In fact, when XCI is induced by inhibiting *Tsix* transcription during differentiation of ESCs into NPCs, the genes in the Xtreme region of the Xi escape XCI (Marks et al., 2015), although these genes are not considered as canonical escapee genes (Berletch et al., 2015; Carrel and Willard, 2005; Li et al., 2012). Heterochromatin structure on the Xi requires repeated maintenance by regenerating heterochromatin after each DNA replication (Allshire and Madhani, 2018). If the Xtreme region is intrinsically less compact, it may become more susceptible to reactivation of the resident genes because of accelerated DNA replication and cell division at the MET stage of reprogramming (Plath and Lowry, 2011).

Although *Gpkow*, *Wdr45*, *Gm45208*, *Tfe3*, *Hdac6*, *Wdr13*, and *Ftsj1* in the Xtreme region show early XCR, we note that not all genes in this region are reactivated early. Thus, in addition to regulation by changes in gross chromatin structure, each gene should be regulated individually, probably via epigenetic regulation such as histone modifications. Indeed, active removal of H3K27me3 and deposition of H3K4me3 correlate with reversal of imprinted XCI (Borensztein et al., 2017), and HDAC1/3 inhibitor enhances XCR, likely via enhanced acetylation of histones (Janiszewski et al., 2019). Our demonstration of dynamic changes in KDM1A occupancy also points to a role for histone modifications in early-onset reactivation on the Xi. KDM1A apparently substitutes some inhibitory mechanism, such as a repressive chromatin structure, and takes over a predominant role in maintaining gene repression. If this shift in repressive mechanism occurs, it would render the Xtreme region more dependent on KDM1A than other regions of the Xi. Subsequent removal of KDM1A from the regulatory regions correlates with reactivation of *Gpkow*, *Wdr45*, *Gm45208*, *Tfe3*, *Hdac6*, *Wdr13*, and *Ftsj1*, where KDM1A occupancy is frequently observed in ESCs (Figure S6C). Consistent with this possible role of KDM1A, the Xi was reported to lack H3K4 methylations, including H3K4me1 and H3K4me2, which are demethylated by KDM1A (Heard et al., 2001; Rens et al., 2010). Thus, restoration of H3K4me2 by either removal or inhibition of KDM1A is expected to play an important role in reactivating genes during XCR.

EXPERIMENTAL PROCEDURES

XCR induction by reprogramming

HAT-bsMEFs were reprogrammed by infection with SeVdp (fK-OSM) including blasticidin S-resistant gene at 32°C for 14 h, as described previously (Nishimura et al., 2014). To minimize contamination of feeder cells, feeder cells were removed by addition of 1 μg/mL of blasticidin S (Wako) 2 days before harvesting the cells. For knockdown of a gene, HAT-bsMEFs were transduced with a retroviral vector expressing shRNA against each target gene for 2 days, followed by selection of the infected cells by 1 μg/mL puromycin. To inhibit the enzymatic activity of KDM1A, HAT-bsMEFs were cultured in the presence of 5 μM of TCP hydrochloride (Abcam) from 7 days before reprogramming.

Determination of allele-specific transcripts by qRT-PCR using TaqMan probes

To quantify relative amount of allele-specific transcripts, standard cDNAs and mixtures of B6 cDNA and Sp cDNA in various ratios were prepared by mixing each cDNA at B6/Sp = 1:99, 20:80, 50:50, 66:33, or 99:1 by copy number. For the standard curve, $\log_2$(Sp cDNA copy number/B6 cDNA copy number) and $\log_2$ (FAM ΔRn/VIC ΔRn) were plotted on the x and y axes, respectively

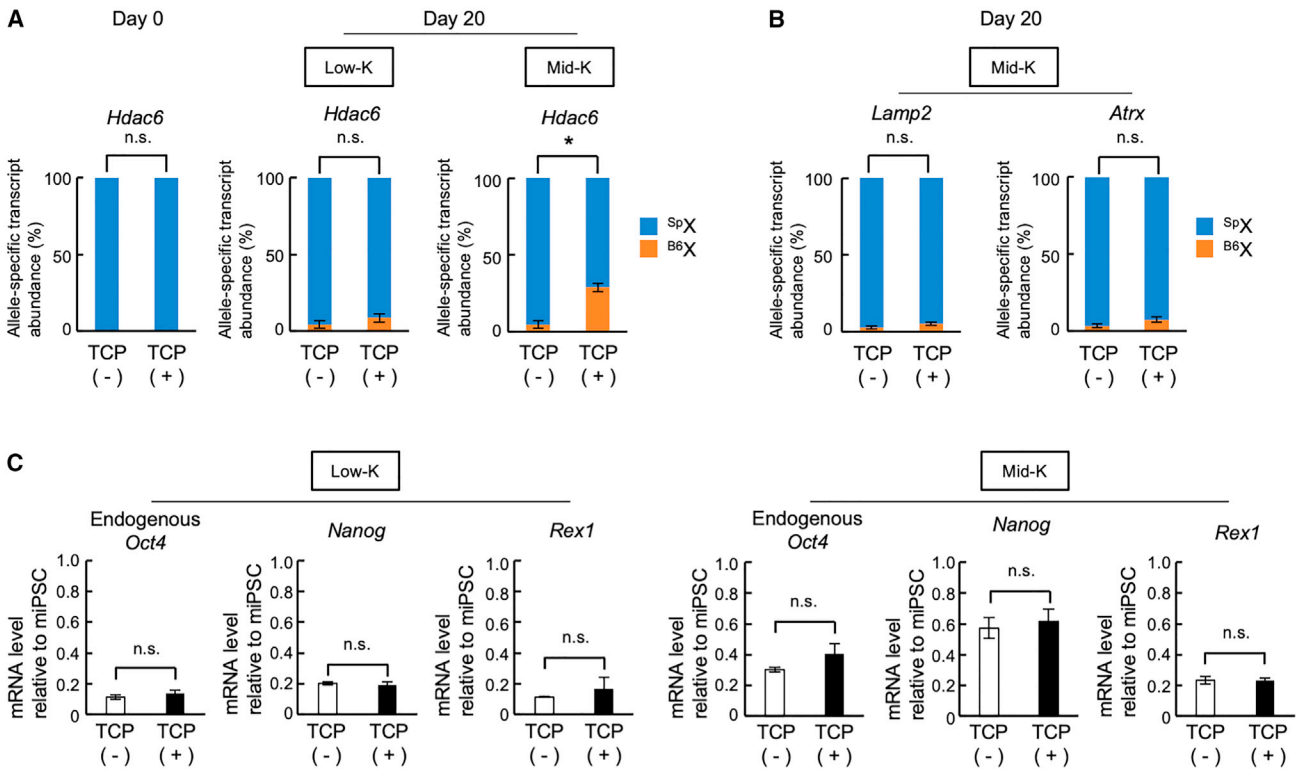

Figure 7. Enhanced transcriptional reactivation on the Xi by a KDM1A inhibitor, TCP

(A and B) Effect of TCP on the transcriptional reactivation of the Xi. HAT-bsMEFs were reprogrammed under the Low-K or Mid-K condition with or without 5 μM TCP. Abundance of allele-specific *Hdac6* transcripts at days 0 and 20 of reprogramming (A) and *Lamp2* and *Atrx* transcripts at day 20 of reprogramming (B) were determined using qRT-PCR with TaqMan probes.

(C) Effect of TCP on induction of pluripotency markers. Endogenous *Oct4*, *Nanog*, and *Rex1* mRNA levels were determined at day 20 of reprogramming as described in (A).

All data represent mean ± SEM of at least three independent experiments. *$p < 0.05$. n.s., not significant.

(Lo et al., 2003). qPCR was performed using TaqMan Genotyping Master Mix (Thermo Fisher Scientific) using the "Genotyping" method in QuantStudio 5 Real-Time PCR System (Thermo Fisher Scientific), following a modified program: the pre- and post-PCR read was done at 25°C. The cycle number was increased to 60 cycles when the target was *Hdac6*. The sequences of the primers and probes are listed in Table S1.

Determination of allele-specific transcripts using RNA-seq

Variant calling was performed using the Basic Variant Call tool in CLC Genomics Workbench version 10.1.1 (Qiagen) to obtain a list of SNP positions and allele frequencies of variants in the RNA-seq reads. The B6 reference read was defined as a read aligned to the reference genome (mm10). The Sp variant read was defined as a read not assigned to the reference genome. To distinguish sequence errors from true polymorphisms, only variants found in more than two samples were classified as polymorphisms between B6 and Sp. At each polymorphism, B6 and Sp allele frequencies were calculated as B6 reference read number/(B6 reference read number + Sp variant read number) and Sp variant read number/(B6 reference read number + Sp variant read number), respectively. B6 gene frequency was calculated as an average of B6 allele frequencies of all polymorphisms in the gene. For clustering according to the B6 gene frequency profile, we used Ward's agglomerative hierarchical clustering on the basis of a Euclidean distance matrix computed using the standard R functions hclust() with method = "ward.D2" and dist() with method = "euclidean." Data at each time point were derived from a single sample.

Single-cell analysis of allele-specific expression

Cells were dissociated with 0.5 g/L trypsin-EDTA (Nacalai Tesque) and suspended in culture medium. Dissociated cells were subjected to single-cell sorting using MoFlo XDP (Beckman) followed by cDNA synthesis using the RT-RamDA cDNA Synthesis Kit (Toyobo). RT-RamDA cDNAs were prepared from 32 and 24 single cells of MEFs and reprogrammed cells, respectively, and only RT-RamDA cDNAs in which *Tbp* expression was detected using qPCR were used for further experiments. For *Tbp* and *Xist* RNA detection, one-fifth the amount of cDNA was used for qPCR analyses. For allele-specific detection using the TaqMan probe, one-fifth the amount of RT-RamDA cDNA was pre-amplified by PCR using AmpliTaq Gold 360 Mastermix

with the primers listed in Table S1. PCR cycles for pre-amplification were as follows: 16 cycles for *Lamp2*, 20 cycles for *Atrx*, and 30 cycles for *Hdac6*. Then, one-fifth the amount of pre-amplified PCR products were used for qPCR with the TaqMan probe. Cells that exhibited more than 25% of the B6 allele-specific transcript abundance were regarded to show transcriptional reactivation of the gene on the Xi.

Statistical analysis

Student's t tests were used to test for statistical significance difference between datasets. A p value < 0.05 was considered to indicate statistical significance.

Data and code availability

The accession number for the RNA-seq and ChIP-seq datasets reported in this paper is GSE157484.

SUPPLEMENTAL INFORMATION

Supplemental information can be found online at https://doi.org/10.1016/j.stemcr.2021.11.008.

AUTHOR CONTRIBUTIONS

S.A., K.N., and K.H. designed the research. S.A., K.N., P.L.B., Y.T.H.T., M.M., T.N., A.S., E.S., and T.S. collected and analyzed the data. S.A., K.N., G.S.M., A. Kuno, M.M., and Y.H. performed the bioinformatic analyses. S.A., A. Kumar, and S.K. prepared the materials. S.A., K.N., A.F., and K.H. wrote the paper.

CONFLICT OF INTERESTS

The authors declare no competing interests.

ACKNOWLEDGMENTS

Hprt-KO *Mus musculus* (RBRC02467) and *Mus spretus* (RBRC00208) were provided by the RIKEN BioResource Research Center (BRC), which is participating in National Bio-Resources Project of the Ministry of Education, Culture, Sports, Science and Technology (MEXT) of Japan. We thank Dr. M. Katsuki for producing the *Hprt*-KO *Mus musculus* strain. This work was funded by Japan Society for the Promotion of Science (JSPS) KAKENHI grants JP19J11416 (S.A), JP16K07244 (K.N.), JP19H03203 (K.N.), JP19K22945 (K.N.), JP19K07343 (A.F.), JP17H05063 (Y.H.), JP17H04036 (K.H.), and JP21H02678 (K.H.), and the Takeda Science Foundation (K.N.). We are grateful to Y. Yamazaki and T. Nishimura for technical assistance with cell sorting and data collection, respectively.

Received: November 16, 2020
Revised: November 16, 2021
Accepted: November 16, 2021
Published: December 16, 2021

REFERENCES

Allshire, R.C., and Madhani, H.D. (2018). Ten principles of heterochromatin formation and function. Nat. Rev. Mol. Cell Biol. *19*, 229–244.

Banaszynski, L.A., Chen, L., Maynard-Smith, L.A., Ooi, A.G.L., and Wandless, T.J. (2006). A rapid, reversible, and tunable method to regulate protein function in living cells using synthetic small molecules. Cell *126*, 995–1004.

Barrero, M.J., Boué, S., and Izpisúa Belmonte, J.C. (2010). Epigenetic mechanisms that regulate cell identity. Cell Stem Cell *7*, 565–570.

Berletch, J.B., Ma, W., Yang, F., Shendure, J., Noble, W.S., Disteche, C.M., and Deng, X. (2015). Escape from X inactivation varies in mouse tissues. PLoS Genet. *11*, 1–26.

Borensztein, M., Okamoto, I., Syx, L., Guilbaud, G., Picard, C., Ancelin, K., Galupa, R., Diabangouaya, P., Servant, N., Barillot, E., et al. (2017). Contribution of epigenetic landscapes and transcription factors to X-chromosome reactivation in the inner cell mass. Nat. Commun. *8*, 1297–1310.

Brown, C.J., and Willard, H.F. (1994). The human X-inactivation centre is not required for maintenance of X-chromosome inactivation. Nature *368*, 154–156.

Brown, C.J., Ballabio, A., Rupert, J.L., Lafreniere, R.G., Grompe, M., Tonlorenzi, R., and Willard, H.F. (1991). A gene from the region of the human X inactivation centre is expressed exclusively from the inactive X chromosome. Nature *349*, 38–44.

Carrel, L., and Willard, H.F. (2005). X-inactivation profile reveals extensive variability in X-linked gene expression in females. Nature *434*, 400–404.

Chaumeil, J., Okamoto, I., and Heard, E. (2003). X-chromosome inactivation in mouse embryonic stem cells: analysis of histone modifications and transcriptional activity using immunofluorescence and FISH. Methods Enzymol. *376*, 405–419.

Csankovszki, G., Panning, B., Bates, B., Pehrson, J.R., and Jaenisch, R. (1999). Conditional deletion of *Xist* disrupts histone macroH2A location but not maintenance of X inactivation. Nat. Genet. *22*, 323–324.

Csankovszki, G., Nagy, A., and Jaenisch, R. (2001). Synergism of Xist RNA, DNA methylation, and histone hypoacetylation in maintaining X chromosome inactivation. J. Cell Biol. *153*, 773–783.

Do, J.T., Han, D.W., Gentile, L., Sobek-Klocke, I., Stehling, M., and Schöler, H.R. (2008). Enhanced reprogramming of Xist by induced upregulation of Tsix and Dnmt3a. Stem Cells *26*, 2821–2831.

Eggan, K., Akutsu, H., Hochedlinger, K., Rideout, W., Yanagimachi, R., and Jaenisch, R. (2000). X-Chromosome inactivation in cloned mouse embryos. Science *290*, 1578–1581.

Engreitz, J.M., Pandya-Jones, A., McDonel, P., Shishkin, A., Sirokman, K., Surka, C., Kadri, S., Xing, J., Goren, A., Lander, E.S., et al. (2013). The Xist lncRNA exploits three-dimensional genome architecture to spread across the X chromosome. Science *341*, 1–9.

Giorgetti, L., Lajoie, B.R., Carter, A.C., Attia, M., Zhan, Y., Xu, J., Chen, C.J., Kaplan, N., Chang, H.Y., Heard, E., et al. (2016). Structural organization of the inactive X chromosome in the mouse. Nature *535*, 575–579.

Hayashi, T., Ozaki, H., Sasagawa, Y., Umeda, M., Danno, H., and Nikaido, I. (2018). Single-cell full-length total RNA sequencing uncovers dynamics of recursive splicing and enhancer RNAs. Nat. Commun. *9*, 619.

Heard, E., Rougeulle, C., Arnaud, D., Avner, P., Allis, C.D., and Spector, D.L. (2001). Methylation of histone H3 at Lys-9 Is an early mark on the X chromosome during X inactivation. Cell *107*, 727–738.

Janiszewski, A., Talon, I., Chappell, J., Collombet, S., Song, J., De Geest, N., To, S.K., Bervoets, G., Marin-bejar, O., Provenzano, C., et al. (2019). Dynamic reversal of random X-Chromosome inactivation during iPSC reprogramming. Genome Res. *29*, 1659–1672.

Kerry, S.B. (2014). Centromeric heterochromatin: the primordial segregation machine. Annu. Rev. Genet. *48*, 457–484.

Kim, J.S., Choi, H.W., Araúzo-Bravo, M.J., Schöler, H.R., and Do, J.T. (2015). Reactivation of the inactive X chromosome and post-transcriptional reprogramming of *Xist* in iPSCs. J. Cell Sci. *128*, 81–87.

Kim, K.Y., Hysolli, E., Tanaka, Y., Wang, B., Jung, Y.W., Pan, X., Weissman, S.M., and Park, I.H. (2014). X chromosome of female cells shows dynamic changes in status during human somatic cell reprogramming. Stem Cell Rep. *2*, 896–909.

Kobayashi, S., Hosoi, Y., Shiura, H., Yamagata, K., Takahashi, S., Fujihara, Y., Kohda, T., Okabe, M., and Ishino, F. (2016). Live imaging of X chromosome reactivation dynamics in early mouse development can discriminate naïve from primed pluripotent stem cells. Development *143*, 2958–2964.

Li, S.M., Valo, Z., Wang, J., Gao, H., Bowers, C.W., and Singer-Sam, J. (2012). Transcriptome-wide survey of mouse CNS-derived cells reveals monoallelic expression within novel gene families. PLoS One *7*, 1–8.

Lo, H.S., Wang, Z., Hu, Y., Yang, H.H., Gere, S., Buetow, K.H., and Lee, M.P. (2003). Allelic variation in gene expression is common in the human genome. Genome Res. *13*, 1855–1862.

Lyon, M.F. (1961). Gene action in the X-chromosome of the mouse (Mus musculus L.). Nature *190*, 372–373.

Maherali, N., Sridharan, R., Xie, W., Utikal, J., Eminli, S., Arnold, K., Stadtfeld, M., Yachechko, R., Tchieu, J., Jaenisch, R., et al. (2007). Directly reprogrammed fibroblasts show global epigenetic remodeling and widespread tissue contribution. Cell Stem Cell *1*, 55–70.

Mahler, K.L., Fleming, J.L., Dworkin, A.M., Gladman, N., Cho, H.Y., Mao, J.H., Balmain, A., and Toland, A.E. (2008). Sequence divergence of Mus spretus and Mus musculus across a skin cancer susceptibility locus. BMC Genomics *9*, 1–12.

Marks, H., Kerstens, H.H.D., Barakat, T.S., Splinter, E., Dirks, R.A.M., van Mierlo, G., Joshi, O., Wang, S.Y., Babak, T., Albers, C.A., et al. (2015). Dynamics of gene silencing during X inactivation using allele-specific RNA-seq. Genome Biol. *16*, 1–20.

Navarro, P., Oldfield, A., Legoupi, J., Festuccia, N., Dubois, A.S., Attia, M., Schoorlemmer, J., Rougeulle, C., Chambers, I., and Avner, P. (2010). Molecular coupling of *Tsix* regulation and pluripotency. Nature *468*, 457–460.

Nichols, J., and Smith, A. (2009). Naive and primed pluripotent states. Cell Stem Cell *4*, 487–492.

Nishimura, K., Sano, M., Ohtaka, M., Furuta, B., Umemura, Y., Nakajima, Y., Ikehara, Y., Kobayashi, T., Segawa, H., Takayasu, S., et al. (2011). Development of defective and persistent Sendai virus vector: a unique gene delivery/expression system ideal for cell reprogramming. J. Biol. Chem. *286*, 4760–4771.

Nishimura, K., Kato, T., Chen, C., Oinam, L., Shiomitsu, E., Ayakawa, D., Ohtaka, M., Fukuda, A., Nakanishi, M., and Hisatake, K. (2014). Manipulation of KLF4 expression generates iPSCs paused at successive stages of reprogramming. Stem Cell Rep. *3*, 915–929.

Okamoto, I., Otte, A.P., Allis, C.D., Reinberg, D., and Heard, E. (2004). Epigenetic dynamics of imprinted X inactivation during early mouse development. Science *303*, 644–649.

Oki, S., Ohta, T., Shioi, G., Hatanaka, H., Ogasawara, O., Okuda, Y., Kawaji, H., Nakaki, R., Sese, J., and Meno, C. (2018). ChIP -Atlas: a data-mining suite powered by full integration of public ChIP -seq data. EMBO Rep. *19*, 1–10.

Pasque, V., and Plath, K. (2015). X chromosome reactivation in reprogramming and in development. Curr. Opin. Cell Biol. *37*, 75–83.

Pasque, V., Karnik, R., Chronis, C., Petrella, P., Langerman, J., Bonora, G., Song, J., Vanheer, L., Dimashkie, A.S., Meissner, A., et al. (2018). X chromosome dosage influences DNA methylation dynamics during reprogramming to mouse iPSCs. Stem Cell Rep. *10*, 1537–1550.

Pasque, V., Tchieu, J., Karnik, R., Uyeda, M., Sadhu Dimashkie, A., Case, D., Papp, B., Bonora, G., Patel, S., Ho, R., et al. (2014). X chromosome reactivation dynamics reveal stages of reprogramming to pluripotency. Cell *159*, 1681–1697.

Plath, K., and Lowry, W.E. (2011). Progress in understanding reprogramming to the induced pluripotent state. Nat. Rev. Genet. *12*, 253–265.

Rens, W., Wallduck, M.S., Lovell, F.L., Ferguson-Smith, M.A., and Ferguson-Smith, A.C. (2010). Epigenetic modifications on X chromosomes in marsupial and monotreme mammals and implications for evolution of dosage compensation. Proc. Natl. Acad. Sci. U S A *107*, 17657–17662.

Sado, T., Wang, Z., Sasaki, H., and Li, E. (2001). Regulation of imprinted X-chromosome inactivation in mice by Tsix. Development *128*, 1275–1286.

Simon, M.D., Pinter, S.F., Fang, R., Sarma, K., Rutenberg-Schoenberg, M., Bowman, S.K., Kesner, B.A., Maier, V.K., Kingston, R.E., and Lee, J.T. (2013). High-resolution Xist binding maps reveal two-step spreading during X-chromosome inactivation. Nature *504*, 465–469.

Skrypek, N., Goossens, S., De Smedt, E., Vandamme, N., and Berx, G. (2017). Epithelial-to-Mesenchymal transition: epigenetic reprogramming driving cellular plasticity. Trends Genet. *33*, 943–959.

Sugimoto, M., and Abe, K. (2007). X chromosome reactivation initiates in nascent primordial germ cells in mice. PLoS Genet. *3*, 1309–1317.

Sun, H., Liang, L., Li, Y., Feng, C., Li, L., Zhang, Y., He, S., Pei, D., Guo, Y., and Zheng, H. (2016). Lysine-specific histone demethylase 1 inhibition promotes reprogramming by facilitating the expression of exogenous transcriptional factors and metabolic switch. Sci. Rep. *6*, 1–14.

Tada, M., Takahama, Y., Abe, K., Nakatsuji, N., and Tada, T. (2001). Nuclear reprogramming of somatic cells by in vitro hybridization with ES cells. Curr. Biol. *11*, 1553–1558.

Takagi, N., Yoshida, M.A., Sugawara, O., and Sasaki, M. (1983). Reversal of X-inactivation in female mouse somatic cells hybridized with murine teratocarcinoma stem cells in vitro. Cell *34*, 1053–1062.

Takahashi, K., and Yamanaka, S. (2013). Induced pluripotent stem cells in medicine and biology. Development *140*, 2457–2461.

Talon, I., Janiszewski, A., Chappell, J., Vanheer, L., and Pasque, V. (2019). Recent advances in understanding the reversal of gene silencing during X chromosome reactivation. Front. Cell Dev. Biol. *7*, 1–13.

Tchieu, J., Kuoy, E., Chin, M.H., Trinh, H., Patterson, M., Sean, P., Aimiuwu, O., Lindgren, A., Hakimian, S., Zack, J.A., et al. (2010). Female human iPS cells retain inactive X-chromosome. Cell Stem Cell *7*, 329–342.

Tomoda, K., Takahashi, K., Leung, K., Okada, A., Narita, M., Yamada, N.A., Eilertson, K.E., Tsang, P., Baba, S., White, M.P., et al. (2012). Derivation conditions impact x-inactivation status in female human induced pluripotent stem cells. Cell Stem Cell *11*, 91–99.

Tran, T.H.Y., Fukuda, A., Aizawa, S., Bui, P.L., Hayashi, Y., Nishimura, K., and Hisatake, K. (2018). Live cell imaging of X chromosome reactivation during somatic cell reprogramming. Biochem. Biophys. Rep. *15*, 86–92.

Vallot, C., Ouimette, J.F., Makhlouf, M., Féraud, O., Pontis, J., Côme, J., Martinat, C., Bennaceur-Griscelli, A., Lalande, M., and Rougeulle, C. (2015). Erosion of X chromosome inactivation in human pluripotent cells initiates with XACT coating and depends on a specific heterochromatin landscape. Cell Stem Cell *16*, 533–546.

Williams, L.H., Kalantry, S., Starmer, J., and Magnuson, T. (2011). Transcription precedes loss of Xist coating and depletion of H3K27me3 during X-chromosome reprogramming in the mouse inner cell mass. Development *138*, 2049–2057.

Yang, F., Babak, T., Shendure, J., and Disteche, C.M. (2010). Global survey of escape from X inactivation by RNA-sequencing in mouse. Genome Res. *20*, 614–622.

Zhang, J., Wheeler, D.A., Yakub, I., Wei, S., Sood, R., Rowe, W., Liu, P.P., Gibbs, R.A., and Bsjetow, K.H. (2005). SNPdetector: a software tool for sensitive accurate SNP detection. PLoS Comput. Biol. *1*, 395–404.

Stem Cell Reports, Volume *17*

Supplemental Information

Early reactivation of clustered genes on the inactive X chromosome during somatic cell reprogramming

Shiho Aizawa, Ken Nishimura, Gonzalo Seminario Mondejar, Arun Kumar, Phuong Linh Bui, Yen Thi Hai Tran, Akihiro Kuno, Masafumi Muratani, Shin Kobayashi, Tsukasa Nabekura, Akira Shibuya, Eiji Sugihara, Taka-Aki Sato, Aya Fukuda, Yohei Hayashi, and Koji Hisatake

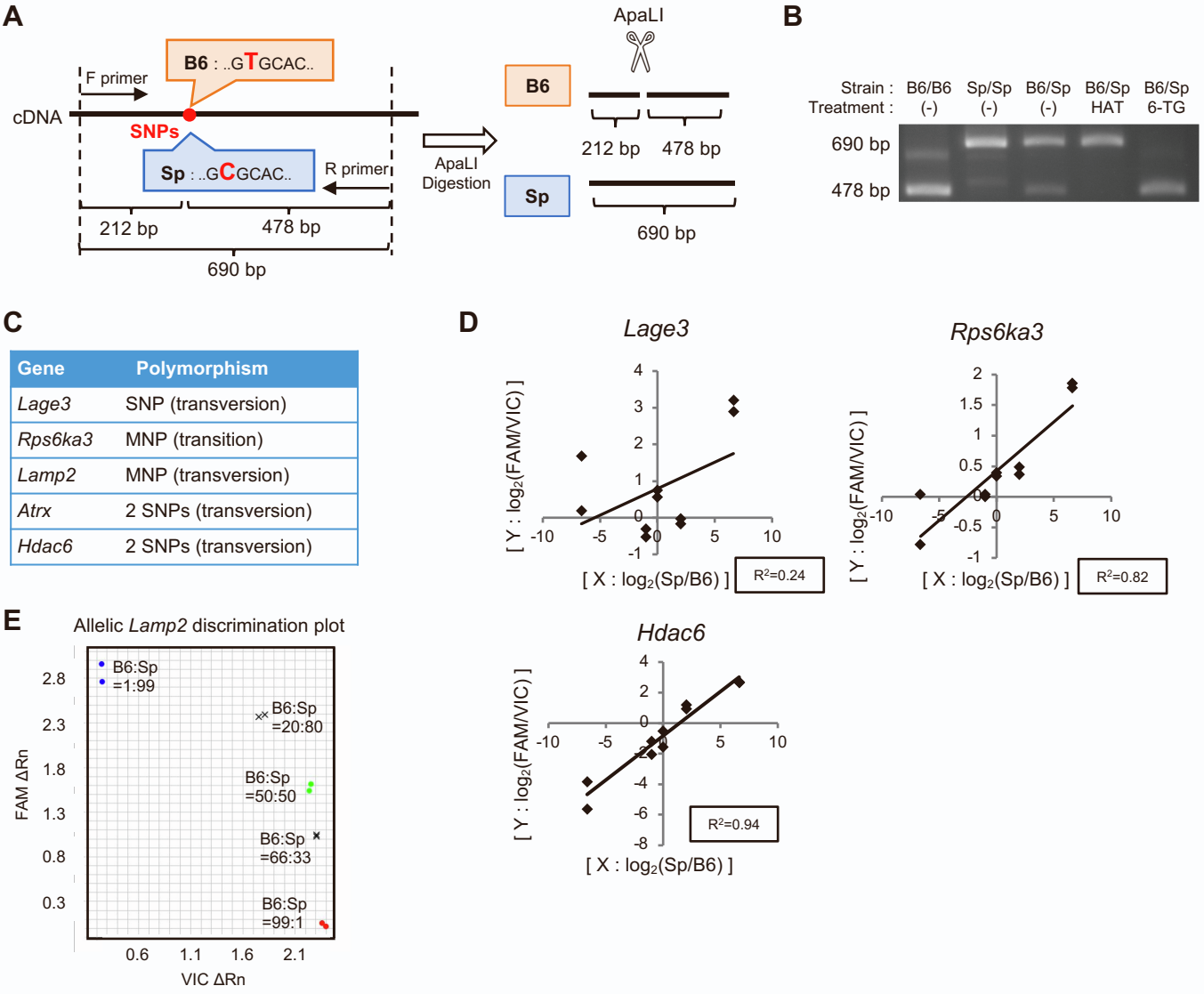

Gene	Polymorphism
Lage3	SNP (transversion)
Rps6ka3	MNP (transition)
Lamp2	MNP (transversion)
Atrx	2 SNPs (transversion)
Hdac6	2 SNPs (transversion)

Figure S1. Detection and determination of allele-specific transcription. Related to Figures 1 and 3

(A) Experimental scheme of *Apa*LI digestion of amplified DNA to distinguish *Lamp2* alleles. cDNA was synthesized from RNA extracted from bsMEFs, and a 690-bp region encompassing the SNP was amplified by PCR from the cDNA. *Apa*LI digests only PCR products from the B6 allele, which produces two shorter fragments. (B) Evaluation of HAT and 6-TG selections by *Apa*LI digestion. cDNA from RNAs extracted from bsMEFs treated with either HAT or 6-TG for 14-20 days, were used for *Apa*LI digestion as described in (A). Fragments were separated by agarose gel electrophoresis. The 690-bp fragment derives from the Sp allele while the 478-bp fragment derives from the B6 allele. (C) Polymorphisms in *Lage3*, *Rps6ka3*, *Lamp2*, *Atrx,* and *Hdac6*, for which TaqMan probes were tested. (D) Graphic plots of abundance of allele-specific transcripts and the proportions of two fluorescence intensities for *Lage3*, *Rps6ka3*, *Atrx,* and *Hdac6*. cDNAs derived from homozygous B6 and Sp mice were mixed at five different ratios (B6 : Sp = 1 : 99, 20 : 80, 50 : 50, 66 : 33, 99 : 1), and qRT-PCR was performed with TaqMan probes for indicated genes. R^2 indicates the square of the correlation coefficient between $\log_2$ of (FAM intensity / VIC intensity) and $\log_2$ of (Sp allelic abundance / B6 allelic abundance). (E) Discrimination of allele-specific *Lamp2* transcripts. cDNAs derived from homozygous B6 and Sp mice were mixed as (D), and qRT-PCR was performed with TaqMan probes for the *Lamp2* gene. VIC ΔRn and FAM ΔRn were plotted on the X and Y axes, respectively. ΔRn means normalized intensity of gained fluorescence for each reporter dye.

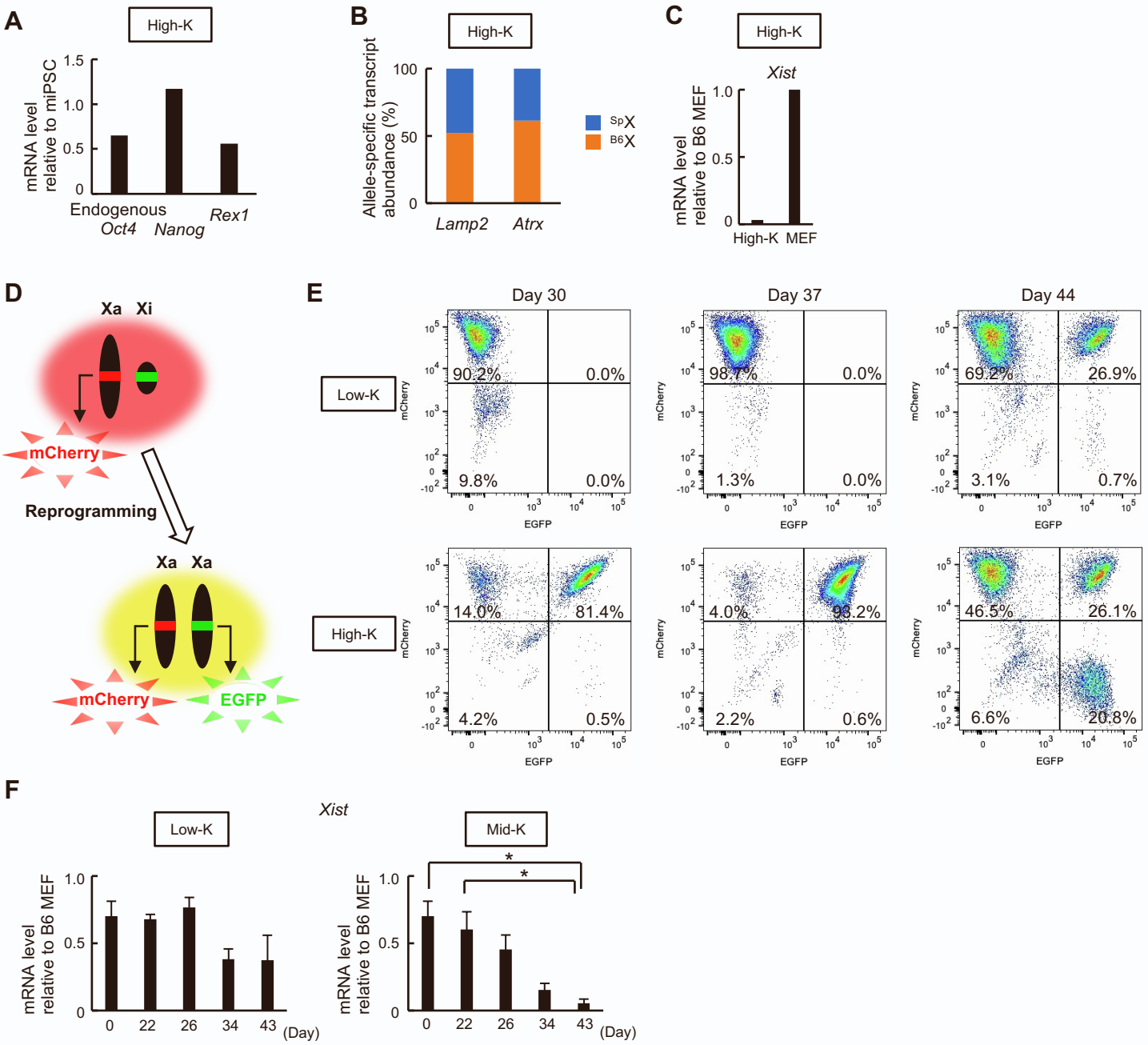

Figure S2. Induction of XCR under the High-K condition. Related to Figure 2

(A) Expression of pluripotency markers in HAT-bsMEFs reprogrammed under the High-K condition. The levels of endogenous *Oct4*, *Nanog*, and *Rex1* mRNA were determined by qRT-PCR at day 30 of reprogramming. Data consist of a single experiment. (B) Relative abundance of allele-specific transcripts in HAT-bsMEFs reprogrammed under the High-K condition. Relative abundance of *Lamp2* and *Atrx* transcripts were determined by TaqMan probes for each gene in the same cells as (A). Data consist of a single experiment. (C) *Xist* RNA levels in HAT-bsMEFs reprogrammed under the High-K condition. The cells described in (A) as well as MEFs were used for qRT-PCR. Data consist of a single experiment. (D) Monitoring of XCR during reprogramming of Momiji mouse-derived MEFs, in which the mCherry or GFP gene was integrated into each allele of *Hprt*. In addition to mCherry expressed from the Xa, reprogrammed mCherry(+) MEFs express GFP from the reactivated Xi. (E) Instability of XCR when iPSCs are fully reprogrammed. mCherry(+) Momiji MEFs were reprogrammed under the Low-K or High-K condition, and fluorescence was observed by FACS at indicated days of reprogramming. (F) Kinetics of the expression level of *Xist* RNA during reprogramming. The expression level of *Xist* RNA was determined by qRT-PCR from the same cells described in Figure 2B. Data represent means ± SEM of at least three independent experiments. *p < 0.05.

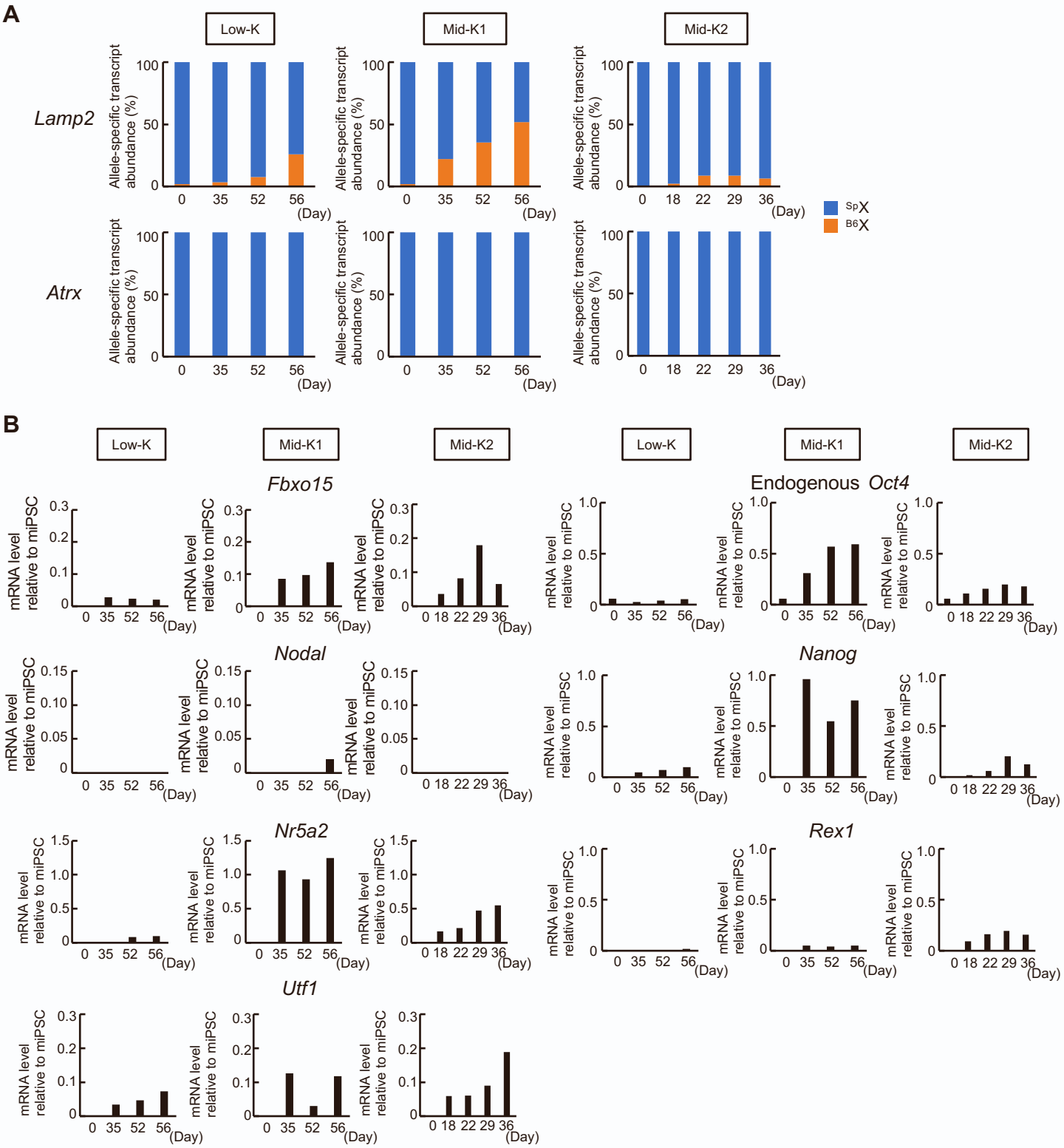

Figure S3. Reactivation of X-linked genes on the Xi in partially reprogrammed iPSCs analyzed in RNA-seq. Related to Figure 3

(A) Relative abundance of allele-specific transcripts of *Lamp2* and *Atrx*. HAT-bsMEFs were reprogrammed under the Low-K and Mid-K conditions, and allele-specific transcripts were analyzed by TaqMan probes for *Lamp2* and *Atrx* at indicated days of reprogramming.
(B) Expression kinetics of pluripotency markers in partially reprogrammed iPSCs. The levels of *Fbxo15, Nodal, Nr5a2, Utf1*, endogenous *Oct4*, *Nanog*, and *Rex1* transcripts in the same cells prepared in (A) were determined by qRT-PCR at indicated days of reprogramming.
All data consist of a single experiment.

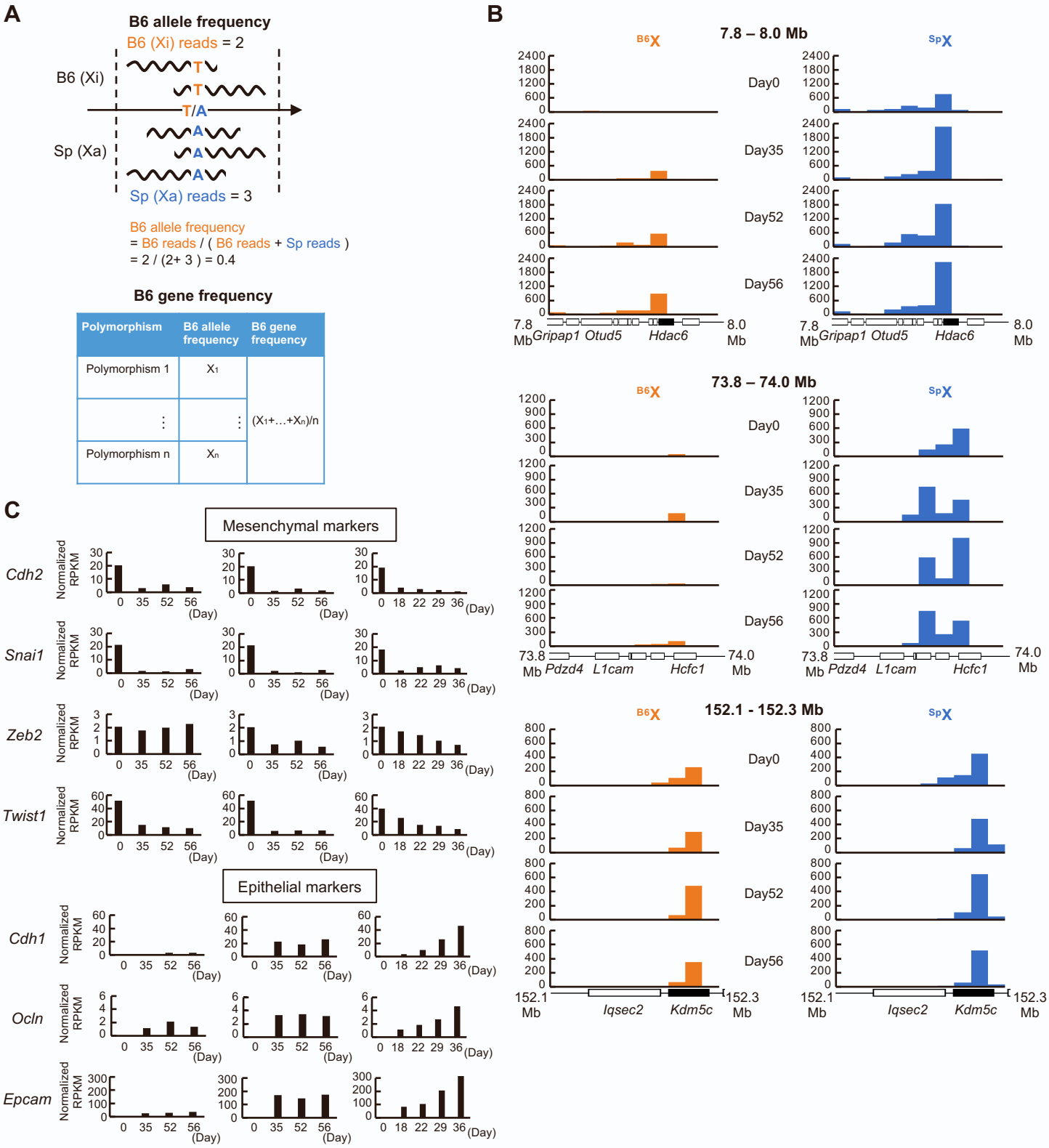

Figure S4. Gene expression data from RNA-seq analyses. Related to Figure 3

(A) Calculation of B6 allele frequency and B6 gene frequency from RNA-seq data. DNA sequence of B6 mouse genome was used as the reference genome. The reads which cannot be aligned to the B6 reference genome were assigned as an Sp-derived transcript. B6 allele frequency is calculated as the number of B6 reads / the number of total reads at each polymorphic position. B6 gene frequency is the average of B6 allele frequencies at all polymorphic positions in the gene. (B) Transcripts from B6 and Sp alleles in representative regions where transcription from the Xi showed increase (7.8-8.0 Mb region: Xtreme) or little change (73.8-74.0 Mb region). A region of an escapee gene is also shown (152.1-152.3 Mb region). Location of *Hdac6* (one of the 7 genes) and *Kdm5c* (escapee) are highlighted. Reads from Mid-K1 cells were assigned to B6 or Sp allele, and the assigned reads were summed up in a 20-kbp window. (C) Kinetics of gene expression of mesenchymal and epithelial markers. Normalized expression values were determined by RNA-seq.

HAT-bsMEF (n=10)

Cell	Abundance of allele-specific transcripts						*Xist* expression level relative to control MEF
	Hdac6		*Lamp2*		*Atrx*		
	B6	Sp	B6	Sp	B6	Sp	
#1	6.3	93.7	0.0	100.0	0.0	100.0	5.471
#2	0.1	99.9	0.0	100.0	0.0	100.0	5.183
#3	0.0	100.0	0.0	100.0	0.0	100.0	4.007
#4	0.1	99.9	0.0	100.0	0.0	100.0	2.653
#5	15.2	84.8	19.5	80.5	0.0	100.0	0.609
#6	0.8	99.2	0.0	100.0	0.0	100.0	2.651
#7	1.1	98.9	0.0	100.0	0.0	100.0	2.771
#8	0.0	100.0	0.0	100.0	0.0	100.0	3.684
#9	22.1	77.9	0.1	99.9	7.0	93.0	2.437
#10	18.9	81.1	0.0	100.0	0.0	100.0	1.053

Mid-K Day 26 (n=16)

Cell	Abundance of allele-specific transcripts						*Xist* expression level relative to control MEF
	Hdac6		*Lamp2*		*Atrx*		
	B6	Sp	B6	Sp	B6	Sp	
#1	5.5	94.5	0.0	100.0	29.2	70.8	0.000
#2	2.8	97.2	2.0	98.0	1.1	98.9	0.337
#3	23.0	77.0	13.1	86.9	0.0	100.0	0.000
#4	35.1	64.9	0.0	100.0	0.0	100.0	0.113
#5	30.6	69.4	0.0	100.0	4.0	96.0	0.000
#6	56.0	44.0	0.0	100.0	4.6	95.4	0.357
#7	24.9	75.1	28.2	71.8	0.0	100.0	0.549
#8	32.4	67.6	9.2	90.8	11.1	88.9	0.000
#9	33.1	66.9	1.1	98.9	0.8	99.2	0.000
#10	43.0	57.0	73.0	27.0	0.0	100.0	0.029
#11	46.9	53.1	1.0	99.0	10.2	89.8	0.000
#12	0.3	99.7	2.0	98.0	0.0	100.0	0.254
#13	11.8	88.2	21.8	78.2	13.7	86.3	0.000
#14	7.9	92.1	0.0	100.0	0.0	100.0	0.000
#15	41.1	58.9	40.1	59.9	0.0	100.0	0.260
#16	26.7	73.3	0.0	100.0	6.9	93.1	0.000

Mid-K Day 34 (n=13)

Cell	Abundance of allele-specific transcripts						*Xist* expression level relative to control MEF
	Hdac6		*Lamp2*		*Atrx*		
	B6	Sp	B6	Sp	B6	Sp	
#1	22.7	77.3	0.0	100.0	0.0	100.0	0.457
#2	60.8	39.2	22.8	77.2	0.0	100.0	0.337
#3	55.7	44.3	8.3	91.7	1.5	98.5	0.000
#4	24.7	75.3	35.6	64.4	7.2	92.8	0.113
#5	54.2	45.8	0.0	100.0	28.9	71.1	0.277
#6	88.3	11.7	0.0	100.0	8.4	91.6	0.000
#7	43.5	56.5	20.3	79.7	39.9	60.1	0.357
#8	0.2	99.8	42.4	57.6	3.6	96.4	0.000
#9	7.0	93.0	0.0	100.0	0.0	100.0	0.000
#10	45.0	55.0	0.0	100.0	27.0	73.0	0.029
#11	68.8	31.2	0.0	100.0	11.0	89.0	0.000
#12	12.7	87.3	0.0	100.0	0.0	100.0	0.000
#13	55.2	44.8	0.1	99.9	0.0	100.0	0.000

Figure S5. Raw data of transcriptional reactivation on the Xi and *Xist* expression in single cells. Related to Figure 4

HAT-bsMEFs were reprogrammed under the Mid-K condition, and single cells were isolated. Relative abundance of allele-specific transcripts were analyzed as in Figure 4A, using RT-RamDA and the TaqMan probes for *Lamp2*, *Atrx*, and *Hdac6*. More than 25% of the B6-specific transcript is regarded as transcriptional reactivation (highlighted in yellow). *Xist* expression levels were determined by qPCR of the same RT-RamDA products. Cells that showed *Xist* expression are highlighted in yellow.

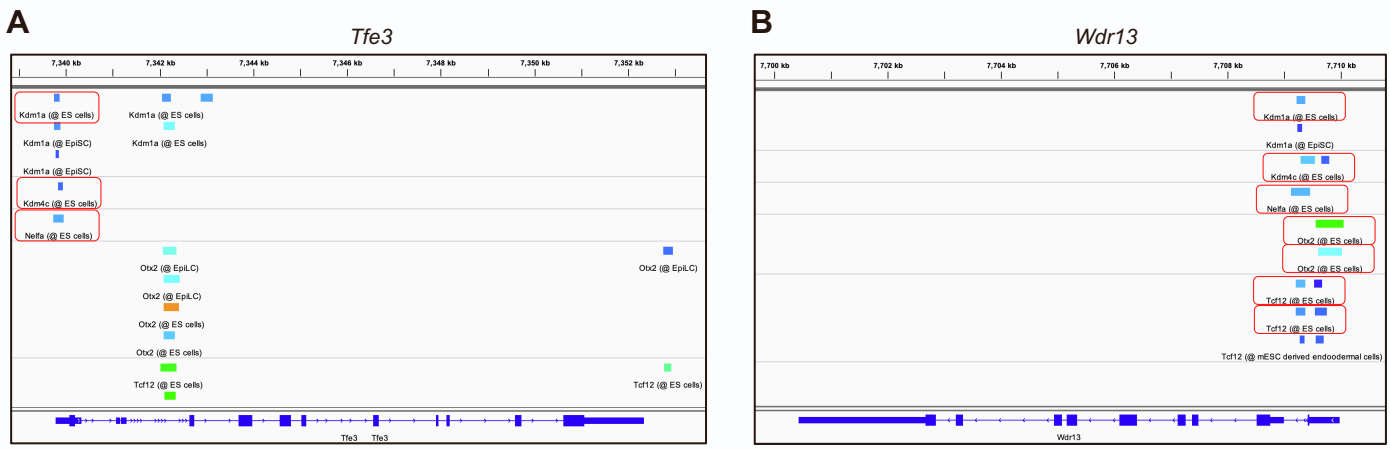

C

Transcriptional regulator	7 genes					
	Gpkow	*Gm45208 /Wdr45*	*Tfe3*	*Hdac6*	*Wdr13*	*Ftsj1*
KDM1A	+		+	+	+	+
KDM4C	+	+	+	+	+	+
NELFA	+	+	+	+	+	+
OTX2		+		+	+	+
TCF12	+	+		+	+	+

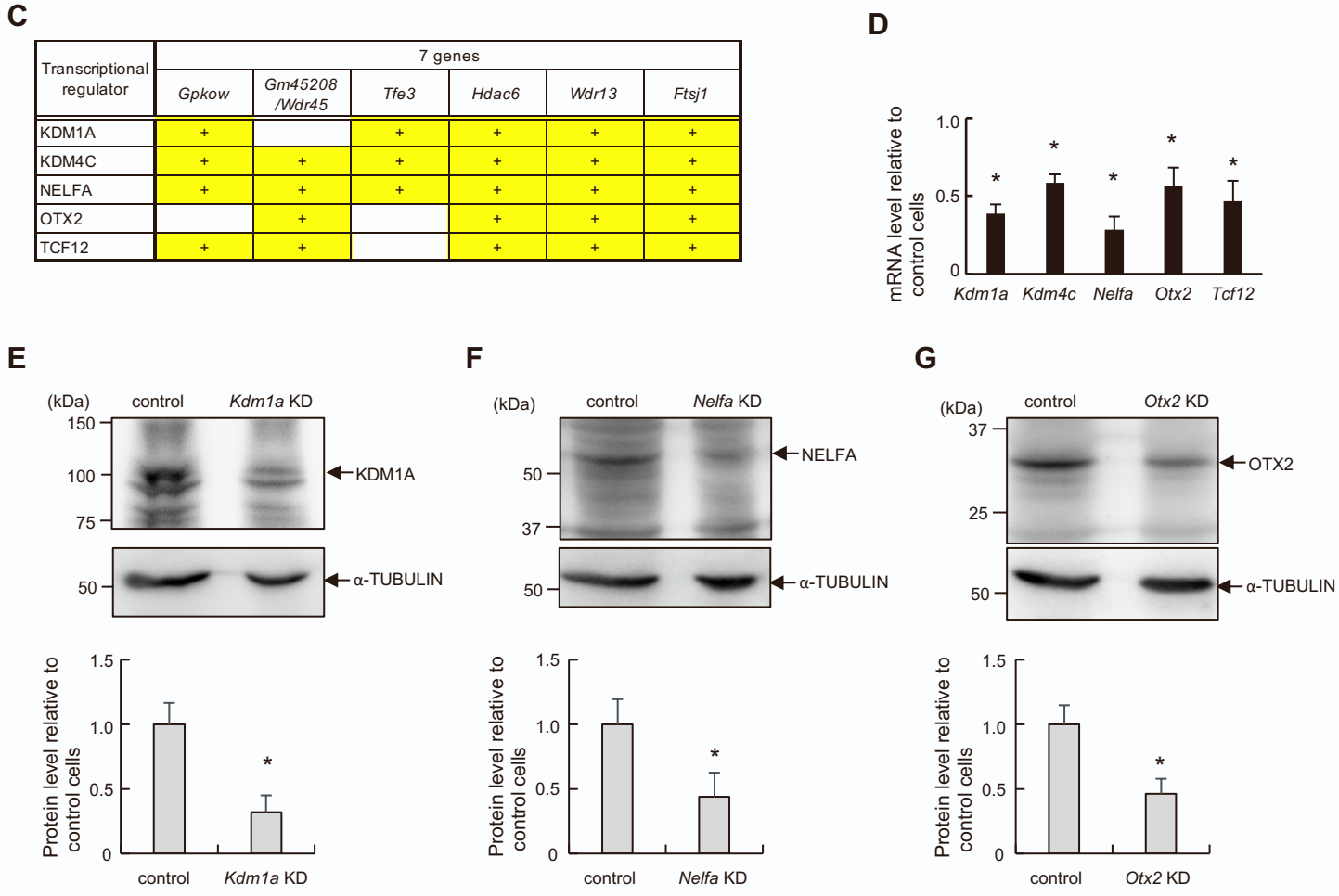

Figure S6. Screening and functional confirmation of candidate transcriptional regulators. Related to Figure 5

(A, B) Representative ChIP-Atlas browser tracks that show occupancies of transcriptional regulators within 1 kb of the TSS of *Tfe3* or *Wdr13* in ESCs. Binding peaks near TSS of *Tfe3* (A) or *Wdr45* (B) in ESCs are enclosed by a red box in the images from ChIP-Atlas peak browser (https://chip-atlas.org/peak_browser). (C) Summary of the occupancies (highlighted in yellow) of transcriptional regulators in the 7 genes. (D) Effect of shRNA on mRNA expression of each transcriptional regulator. The mRNA level was determined in HAT-bsMEFs (*Kdm1a*, *Kdm4c*, *Nelfa*, and *Tcf12*) or bsMEF-derived iPSCs (*Otx2*) after transduction of a retrovirus expressing shRNA against each transcriptional regulator. Data represent means ± SEM of at least three independent experiments. *p < 0.05 versus cells infected with control hKO-expressing retrovirus. (E-G) Effect of shRNA on the protein level of its target gene. MEFs treated with shRNA for *Kdm1a* (E) or *Nelfa* (F) or ESC for *Otx2* (G) were selected by puromycin for 3 days. The protein level was determined using the whole cell extract from the selected cells. The lower graphs show the intensity of each band normalized against α-TUBULIN. Data are represented as means SEM of three independent experiments. *p < 0.05 versus mock infected control cells.

Table S1. Primers and probes used for allele distinction. Related to Figures 1, 2, 3, 4, 5, 6, and 7, and Figures S1, S2, S3, and S5.

Target	Types of oligonucleotide		Sequence
Lamp2	Primers for allele-specific digestion	Forward primer	GGCTCAGCTTTCAACATTTCC
		Reverse primer	GGCATCTTAGGTTAGGATCCCA
	Primers for single cell analysis	Forward primer	TACCTGACAAGGCGACACAC
		Reverse primer	GCACTGCAGTCTTGAGCTGT
	Primer	Forward primer	CACCTGCAAGCTTTTGTCCA
		Reverse primer	GTGTGAATGATGGGTGCCAC
	Probe	B6	AAGACCAAACTccCACCAC
		Sp	AAGACCAAACTgtCACCAC
Atrx	Primers for single cell analysis	Forward primer	CGACGACGACAATGATCCTGA
		Reverse primer	GTGAAGAAAACTAACCACCTGGA
	Primer	Forward primer	GTTCAAGAGGATTCCTCCAGTGA
		Reverse primer	TTCTGCCTTTTCCAGGTGACTT
	Probe	B6	TTCTGAGGAGGAcAAgAA
		Sp	TGAGGAGGAaAAaAA
Hdac6	Primers for single cell analysis	Forward primer	CAGCAGGATTTGCCCACCTA
		Reverse primer	CACGATTAGGATCCGCAGGG
	Primer	Forward primer	CCTTCTGGGAGGTCCTGGA
		Reverse primer	GCTGAGGTGTCTCAGGGTGAT
	Probe	B6	AAGAAGCCgTgCTAGAAG
		Sp	TGGAAGAAGCCaTtCTAGAAG
Rps6ka3	Primer	Forward primer	CCATCCAACATTTTGTATGTTTTTG
		Reverse primer	GCCATCTCTAAGGTTTGCCG
	Probe	B6	TAAATAGTTCACctGGATTAA
		Sp	TAAATAGTTCACtgGGATTAA
Lage3	Primer	Forward primer	TTTAACCCAAAGGCCTGGAA
		Reverse primer	GCGATTTCTGCCTCCAAAGA
	Probe	B6	ACATCACAGATTCtCCCTCT
		Sp	ATCACAGATTCgCCCTCT

Table S2. Primers used for genotyping. Related to Figure 1

Target	Types of primer	Sequence
Zfy1 (chr. Y)	Forward primer	TGGTGATTCAATAATGTCTGTTCAGCTG
	Reverse primer	GGACAAACTTTACGTGTCTATCCTTGC
Hprt	Forward primer	GAGAGAACTGCTACCACTGAGAG
	Reverse primer for *Hprt*(-)	GTTATTGGTGGAGATGATCTCTCAAC
	Reverse primer for *Hprt*(+)	ATCAGAGCAGCCGATTGTCTGTTG

Table S3. Primers used for qRT-PCR. Related to Figures 2, 4, 5, and 7, and Figures S2, S3, and S6

Target	Types of primer	Sequence
Fbxo15	Forward primer	CTCATCTGTCACGAAGCAGC
	Reverse primer	AGGTCACCGCATCCAAGTAA
Kdm1a	Forward primer	CTCCTGGCCCCTCAATTC
	Reverse primer	TGTGTGTTCTCCAGCAAAGAA
Kdm4c	Forward primer	GCGGGTTCATGCAAGTTGTT
	Reverse primer	GTTTCAGAGCACCTCCCCTC
Nanog	Forward primer	ACCTGAGCTATAAGCAGGTTAAGAC
	Reverse primer	GTGCTGAGCCCTTCTGAATCAGAC
Nelfa	Forward primer	CTGGCCTGGTATCCACACAG
	Reverse primer	AGTCTCAGAGCTGGGGATGT
Nodal	Forward primer	ACATGTTGAGCCTCTACCGAG
	Reverse primer	GTGAAAGTCCAGTTCTGTCCG
Nr5a2	Forward primer	CAAAGTGGAGACGGAAGCC
	Reverse primer	ATCGCCACACACAGGACATA
endogenous *Oct4*	Forward primer	CTGTTCCCGTCACTGCTCTG
	Reverse primer	AACCCCAAAGCTCCAGGTTC
Otx2	Forward primer	CTCGACGTTCTGGAAGCTC
	Reverse primer	GGCCTCACTTTGTTCTGACC
Rex1	Forward primer	TTGATGGCTGCGAGAAGAG
	Reverse primer	ACCCAGCCTGAGGACAATC
Tbp	Forward primer	TATCTGCTGGCGGTTTGGC
	Reverse primer	TGAAATAGTGATGCTGGGCAC
Tcf12	Forward primer	AGACACAAACCTGGCAGGAG
	Reverse primer	TGCAGAAGCGACACACTGAT
Utf1	Forward primer	GTCCCTCTCCGCGTTAGC
	Reverse primer	GGGGCAGGTTCGTCATTT
Xist (B6)	Forward primer	GGTTCTCTCTCCAGAAGCTAGGAAAG
	Reverse primer	TGGTAGATGGCATTGTGTATTATATGG

Table S4. Annealed oligos for shRNA. Related to Figure 5 and Figure S6

Target	Sequence
Kdm1a	gatccGAGTTGAAAGAGCTTCTTAATCTCGAGATTAAGAAGCTCTTTCAACTCTTTTTGg
	aattcCAAAAAGAGTTGAAAGAGCTTCTTAATCTCGAGATTAAGAAGCTCTTTCAACTCg
Kdm4c	gatccGCAGAGTGATAGATGTGACATCTCGAGATGTCACATCTATCACTCTGCTTTTTGg
	aattcCAAAAAGCAGAGTGATAGATGTGACATCTCGAGATGTCACATCTATCACTCTGCg
Nelfa	gatccGCCAGTACCTGAACAAGAATGCTCGAGCATTCTTGTTCAGGTACTGGCTTTTTGg
	aattcCAAAAAGCCAGTACCTGAACAAGAATGCTCGAGCATTCTTGTTCAGGTACTGGCg
Otx2	gatccGCATGGACTGTGGATCTTATTCTCGAGAATAAGATCCACAGTCCATGCTTTTTGg
	aattcCAAAAAGCATGGACTGTGGATCTTATTCTCGAGAATAAGATCCACAGTCCATGCg
Tcf12	gatccGAAGGCCTTGGCATCTATTTACTCGAGTAAATAGATGCCAAGGCCTTCTTTTTGg
	aattcCAAAAAGAAGGCCTTGGCATCTATTTACTCGAGTAAATAGATGCCAAGGCCTTCg

SUPPLEMENTAL EXPERIMENTAL PROCEDURES

Isolation and selection of mouse embryonic fibroblasts

Mouse embryonic fibroblasts (MEFs) were derived from E13.5 embryos which were derived from the cross between female *Hprt*-KO *Mus musculus* (RBRC02467, RIKEN Bioresource Center) and male *Mus spretus* (RBRC00208, RIKEN Bioresource Center) and cultured in MEF medium (DMEM (Sigma) supplemented with 10% FBS (Biosera), 100 U/mL penicillin-streptomycin (Nacalai Tesque)). To select bsMEFs ($^{B6}X^{Hprt-}$, ^{Sp}X) from the isolated MEFs, their genomic DNAs were genotyped by PCR using KOD-Plus-Neo (TOYOBO). Genomic DNAs were extracted using Geno Plus Mini (VIOGENE). DNA sequences of the PCR primers are shown in Table S2.

In order to isolate subpopulations of 6TG-bsMEF (^{B6}Xa, ^{Sp}Xi) from bsMEF, the cells were cultured in MEF medium containing 40 mM of 6-TG (Sigma) for 14 days. For isolating HAT-bsMEFs (^{B6}Xi, ^{Sp}Xa), bsMEFs were cultured in HAT medium (MEF medium supplemented with 4 mg/mL Hypothanthine (Sigma), 2 mg/mL Thymidine (Sigma) and 1 μg/mL MTX (Pfizer)) for 14-20 days. Because Momiji MEFs (Kobayashi et al. 2016) possess GFP and mCherry at each allele of the *Hprt* locus, the MEFs were sorted by MoFlo XDP (Beckman coulter) to isolate a homogeneous population of mCherry(+) MEFs.

Detection of allele-specific transcripts by PCR

For allele-specific digestion, PCR was done to amplify cDNA of the *Lamp2* transcript using KOD-plus-neo. The PCR products were then digested by ApaLI (New England Biolabs) at 37˚C for 1 hour and analyzed on an agarose gel. The DNA sequences of the used primers are listed in Table S1.

Design of TaqMan probes for determination of allele-specific transcripts

TaqMan probes were designed based upon polymorphisms between B6 and Sp, which were available from Sanger Mouse Genomes Project. Target polymorphisms were chosen according to the following criteria: 1) one MNP or two SNPs that can be included in a single probe and 2) MNP or SNPs that are located within genes expressed both in MEFs and ESCs. Custom TaqMan SNP Genotyping Assays (Thermo Fisher) was used to create the probes labeled with a fluorescence reporter (VIC for B6 allele or FAM for Sp allele) and NFQ-MGB quencher.

SeVdp vector production

Blasticidin S-resistant gene together with the T2A peptide sequence was amplified and inserted after the c-MYC-coding sequence of SeVdp(fK-OSM). SeVdp vectors were produced as described previously (Nishimura et al. 2011). Titers of the SeVdp vectors were determined by

counting the number of NIH3T3 cells infected with serial dilutions of vector suspension, using immunostaining with an anti-SeV NP antibody (Nishimura et al. 2007).

cDNA synthesis and qPCR

Total RNA was extracted using ISOGEN (Nippon Gene). RNA concentration was measured by Nanodrop 2000 (Thermo Fisher). Reverse transcription was performed using Superscript III First-Strand Synthesis System (Thermo Fisher). Quantitative PCR (qPCR) was performed using QuantStudio 5 Real-Time PCR System (Applied Biosystems) with GoTaq qPCR Master Mix (Promega). As controls, we used cDNA from germline-competent mouse iPSCs generated by the SeVdp vector (Nishimura et al. 2011). The expression levels were normalized against that of TATA-box binding protein (*Tbp*). The DNA sequences of the primers are listed in Table S3.

Fluorescence activated cell sorting (FACS) for monitoring of XCR

Expression of mCherry and EGFP from reprogrammed Momiji MEFs were detected by FACS Aria SORP (BD Biosciences) with 530/30 nm and 610/20 nm fluorescent filters. Data were analyzed using FlowJo software (BD Biosciences).

RNA-seq

RNA concentration was measured by Nanodrop 2000 (Thermo Fisher), and RNA quality was validated with RNA 6000 Pico kit (Agilent). RNA-seq libraries were constructed with 500 ng of total RNA using NEBNext Poly(A) mRNA Magnetic Isolation Module and NEBNext Ultra Directional RNA Library Prep Kit (New England Biolabs). Sequencing was performed with NextSeq 500 (Illumina) with paired-end mode for 2x76-base reads. FASTQ files were imported to CLC Genomics Workbench (CLC-GW, Version 10.1.1, Qiagen). Mapping to the mouse reference genome (mm10) was performed with RNA-seq analysis tool in CLC-GW. Transcription expression values were obtained in RPKM (reads per kilobase per million reads) and normalized by quantile normalization method.

Analyses of published data

To analyze ATAC-seq data of GSM1828645 and GSM1828646 (Giorgetti et al. 2016) annotated to the mouse reference genome (mm9), all peaks were shifted to mm10 using Lift Genome Annotations (https://genome.ucsc.edu/cgi-bin/hgLiftOver). Relative accessibility of Xi was calculated as 129 (Xi) reads / Cast (Xa) reads in each polymorphism. To compare chromatin accessibility in regions in the Xi, all of 129 (Xi) reads were summed up in 2-Mbs windows.

To screen for candidate factors that bind the Xtreme region, peak information was visualized and retrieved from ChIP-Atlas database using Peak Browser (Oki et al. 2018). All proteins in “TFs

and others" (332 factors out of 13,558 data sets) that show binding within ±1 kbs of TSSs of *Gpkow*, *Gm45208*/*Wdr45*, *Tfe3*, *Hdac6*, *Wdr13* and *Ftsj1* in "Embryonic Stem Cells" of "Pluripotent stem cell" were screened. The proteins that show binding to more than 5 genes were selected as candidate transcriptional regulators potentially relevant to early-onset reactivation on the Xi.

Production of retroviral vector

To prevent retrovirus silencing during reprogramming, the shRNA expression cassette from pMXs-U6-Puro plasmid (Cambridge bioscience) was inserted into pMCsΔYY1-IRES-Puro plasmid (Nishimura et al. 2017) to produce pMCΔYY-U6-Puro plasmid. Annealed DNA oligonucleotides were inserted into pMCΔYY-U6-Puro to construct the retroviral vector expressing shRNA against each target gene. The DNA sequences of the annealed DNA oligonucleotides are listed in Table S4.

PLAT-E cells were transfected with each vector using Lipofectamine 2000 (Thermo Fisher). Viral supernatant was collected 2 days after transfection and filtered through a 0.45 μm cellulose acetate filter and stored at -80 ˚C until use.

Determination of Protein Expression by Immunoblotting

MEFs or EB5 mESCs transduced with shRNA-expressing retroviral vector were collected three days after puromycin treatment, and proteins from these cells were isolated as described previously (Bui et al. 2019). Protein expression levels were quantified using FUSION FX7.EDGE and FUSION Capt Software (Vilber-Lourmat). We employed the following primary antibodies; anti-KDM1A/LSD1 (1:2,000, ab17721; Abcam), anti-NELFA (1:2,000, 10456-1-AP; Proteintech), anti-OTX2 (1:2,000, GTX133210; GeneTex), and anti-α-TUBULIN (1:10,000, ab7291; Abcam).

ChIP-seq and calculation of KDM1A occupancy

Chromatin immunoprecipitation was done as described previously (Nishimura et al., 2017) using anti-KDM1A/LSD1 (ab17721; Abcam). Libraries for ChIP-seq were prepared using KAPA HyperPlus Kit (Roche) according to the manufacturer's instructions. Briefly, 10 ng of ChIP DNA was used for library preparation with unique dual index adaptor from IDT for Illumina TruSeq DNA UD Indexes (Illumina). The libraries were quantified using Qubit 4 Fluorometer (Thermo Fisher) and analyzed for size distribution using MultiNA (Shimdzu) or TapeStation 2200 (Agilent Technologies). Paired-end sequencing of the libraries was performed with Novaseq 6000 Sequencing System using SP 100 cycle kit (Illumina).

ChIP-seq reads were mapped to the mouse reference genome (mm10) using BWA-MEM version 0.7.17 (Li and Durbin, 2010). Variant calls were conducted using piping samtools mpileup

output into bcftools call (Li et al., 2009). To remove sequence errors, only variants found in more than two samples were regarded polymorphisms between B6 and Sp. To calculate KDM1A occupancy, all the reads in enhancer, promoter, and gene body was summed up in 0.2 Mb windows. Then, the summed read numbers of the Xi were normalized against that of the Xa. We used ESC enhancers based on EnhancerAtlas 2.0 (Gao and Qian, 2020) (ESC_J1) (http://www.enhanceratlas.org/indexv2.php) as enhancers for the nearest neighbor genes. Reads within ±1 kb from TSS of each gene were assigned as reads for promoter. Data under each condition were derived from a single sample.

SUPPLEMENTAL REFERENCES

Bui, P.L., Nishimura, K., Seminario Mondejar, G., Kumar, A., Aizawa, S., Murano, K., Nagata, K., Hayashi, Y., Fukuda, A., Onuma, Y., et al. (2019). Template Activating Factor-I alpha Regulates Retroviral Silencing during Reprogramming. Cell Rep 29, 1909-1922 e1905.

Gao, T., and Qian, J. (2020). EnhancerAtlas 2.0: An updated resource with enhancer annotation in 586 tissue/cell types across nine species. Nucleic Acids Res. *48*, D58–D64.

Giorgetti L, Lajoie BR, Carter AC, Attia M, Zhan Y, Xu J, Chen CJ, Kaplan N, Chang HY, Heard E, et al. (2016). Structural organization of the inactive X chromosome in the mouse. Nature *535*: 575–579.

Kobayashi S, Hosoi Y, Shiura H, Yamagata K, Takahashi S, Fujihara Y, Kohda T, Okabe M, Ishino F. (2016). Live imaging of X chromosome reactivation dynamics in early mouse development can discriminate naïve from primed pluripotent stem cells. Development *143*: 2958–2964.

Li, H., and Durbin, R. (2010). Fast and accurate long-read alignment with Burrows-Wheeler transform. Bioinformatics *26*, 589–595.

Li, H., Handsaker, B., Wysoker, A., Fennell, T., Ruan, J., Homer, N., Marth, G., Abecasis, G., and Durbin, R. (2009). The Sequence Alignment/Map format and SAMtools. Bioinformatics *25*, 2078–2079.

Nishimura K, Aizawa S, Nugroho FL, Shiomitsu E, Tran YTH, Bui PL, Borisova E, Sakuragi Y, Takada H, Kurisaki A, et al. (2017). A Role for KLF4 in Promoting the Metabolic Shift via TCL1 during Induced Pluripotent Stem Cell Generation. Stem Cell Reports *8*: 787–801.

Nishimura K, Sano M, Ohtaka M, Furuta B, Umemura Y, Nakajima Y, Ikehara Y, Kobayashi T, Segawa H, Takayasu S, et al. (2011). Development of defective and persistent Sendai virus vector: A unique gene delivery/expression system ideal for cell reprogramming. J Biol Chem *286*: 4760–4771.

Nishimura K, Segawa H, Goto T, Morishita M, Masago A, Takahashi H, Ohmiya Y, Sakaguchi T, Asada M, Imamura T, et al. (2007). Persistent and stable gene expression by a cytoplasmic RNA replicon based on a noncytopathic variant sendai virus. J Biol Chem *282*: 27383–27391.